Supporting Information for

Hemicyanine and Its Hexyltriphenyl Borate Ion Pairs as Red and Near IR Light-Absorbing Photoinitiators for Efficient Radical Photopolymerization

Xueqi Qin,[a‡] *Peiwen Jiang*,[a‡] *Greta Sambucari*,[b,g] *Talita Jordanna de Souza Ramos*,[b] *Yuqi Hou*,[c] *Hujun Huang*,[d] *Xin Dong*,[d] *Jianzhang Zhao*,[a,*] *Davy-Louis Versace*,[e,*] and *Mariangela Di Donato*[b,f,*]

[a] State Key Laboratory of Fine Chemicals, Frontiers Science Center for Smart Materials, School of Chemical Engineering, Dalian University of Technology, Dalian 116024, (P. R. China). *E-mail: zhaojzh@dlut.edu.cn (J.Z.)

[b] LENS (European Laboratory for Non-linear Spectroscopy)via N. Carrara 1, 50019 Sesto Fiorentino (FI), Firenze, Italy. *E-mail: didonato@lens.unifi.it

[c] School of Chemical Engineering, Ocean and Life Sciences, Dalian University of Technology, Panjin 124221, P. R. China

[d] Ningbo Sunny Automotive Optech Co. Ltd., No. 27–29 Shunke Road, Ning Bo City, Yuyao 315400, P. R. China

[e] Institut de Chimie et des Matériaux Paris-Est (ICMPE), Université Paris-Est Créteil (UPEC), UMR CNRS 7182 2–8 rue Henri Dunant, 94320 Thiais (France); E-mail: davy-louis.versace@cnrs.fr

[f] ICCOM-CNR,via Madonna del Piano 10,50019 Sesto Firorentino (FI), Italy

[g] INO-CNR, via N. Carrara 1, 50019 Sesto Fiorentino (FI)

‡These authors contributed equally to this work.

Index

1. Experimental section

General Method. Compounds **C-1** ~ **C-4** and **C-1-NB** were prepared according to previously reported methods and were analytically pure.[1-4] Solvents were dried and distilled prior to use. The ^{1}H NMR spectra were recorded with Bruker 400/500 MHz spectrometer, and the solvent was $CDCl_3$ or dimethyl sulfoxide (DMSO-d_6). The UV-Vis absorption spectra of the compounds were determined by UV-2550 spectrophotometer (Shimadzu Ltd., Japan). Fluorescence emission spectra were recorded on the FS5 spectrometer (Edinburgh Instruments, U.K.). The luminescence lifetime was measured using a fluorescence upconversion setup based on a mode-locked Ti-sapphire laser (Mai Tai DeepSee, Spectra-Physics, USA), which served as the excitation source for time-resolved fluorescence spectroscopy.

Electrochemical Studies. The cyclic voltammetry was studied using the CHI610D Electrochemical Workstation (CHI instruments, Inc., Shanghai, China). A platinum counter electrode, glassy carbon working electrode, and $Ag/AgNO_3$ (0.1 M in ACN) reference electrode were used in the measurements, with tetrabutylammonium hexafluorophosphate ($Bu_4N[PF_6]$) as the supporting electrolyte and ferrocenium/ferrocene (Fc^+/Fc) as the internal reference. The sample solutions were purged with N_2 for 15 minutes, and all electrochemical measurements were performed under a N_2 atmosphere.

DFT Calculation. The geometry of the cationic form and the neutral radical of the photoinititors were optimized with restricted and unrestricted DFT, all at the B3LYP 6-31G (d) level using Gaussian 16.[5] The calculation of the spin orbital coupling matrix elements (SOCMEs) of the cyanine dyes were performed at B3LYP/def2-TZVP level using the ORCA 6.0 programs.[6]

Nanosecond Transient Absorption Spectroscopy. Nanosecond transient absorption spectra were measured by LP980 laser flash photolysis Spectrometer (Edinburgh Instruments, U.K.). The transient signals are digitized on the Tektronix TDS 3012B oscilloscope. The sample solutions were purged with N_2 before measurement. The solution excited with a nanosecond pulsed laser (Surelite OPO Plus SL 1-10, Continuum Ltd., USA). The typical energy of the pulsed laser is *ca.* 10 mJ per pulse. L900 software was used for the data analysis.

Femtosecond Transient Absorption Spectroscopy. The femtosecond transient absorption spectra were recorded on a system based on Ti: sapphire regenerative amplifier system (Coherent Legend Elite) emitting laser pulses centered at 800 nm, with 40-fs pulse duration and 1 kHz repetition rate. The wavelength of the pump beam varied between 550 and 620 nm, depending on the specific sample and was produced either as

second harmonic of the signal output of a commercial optical parametric amplifier (TOPAS, Light Conversion) or by mixing the TOPAS signal with residual fundamental radiation at 800 nm. The probe beam was generated by focusing a small portion of the fundamental laser radiation on a 3 mm thick CaF_2 crystal. Pump-probe delays were introduced by sending the portion of the laser beam used for generating the probe through a motorized stage, allowing to change the time of arrival of the probe with respect to the pump in a time interval spanning up to 3.8 ns. The pump and probe beam were both focused and overlapped at the sample position, using spherical mirrors (75 mm focal distance). After crossing the sample, the probe was dispersed using a monochromator and revealed through a home-made silicon array detector. The data were analyzed with a global analysis procedure using the software Glotaran-1.5.1.[7]

Photopolymerization Kinetic Investigations.[8] The real-time infrared spectrum recorded with FT-IR spectrometer (Thermo Scientific Nicolet iS20) was used to continuously track the kinetic traces of the photopolymerization process, and the corresponding LED was used for photoirradiation of the photopolymerization blends, and the irradiation intensity was 1.0 mW/cm^2. The change of double band conversion (DC) with time was determined by monitoring the change of the C=C stretching vibrational absorption peak centered at 1630 cm^{-1} and taking C=O centered at 1760 cm^{-1} as internal standard. The calculation formula is:

$$\text{Conversion (\%)} = \left(1-\frac{A_t}{A_0}\right) \times 100\% \quad (4)$$

where A_0 and A_t represent the ratio of the relative absorption band areas before photopolymerization and at photopolymerization time t, respectively.

2. Synthesis of the compounds

Synthesis of compound 1. This procedure is based on a literature report.[9] Under Nitrogen atmosphere, in ice water, $POCl_3$ (0.4 mL, 4.2 mmol.) was carefully added to anhydrous DMF (4 mL) and the mixture was stirred at 50 °C for 45 min. Then,7-diethyl amino coumarin (600 mg, 3 mmol.) dissolved in anhydrous DMF (3 mL) was added and the reaction mixture was stirred for 2 h at 60 °C. After completion, 100 mL of iced water was added and the mixture was stirred for 1 h until an orange precipitate appeared. The precipitate was filtered and washed twice with water. The crude product was co-evaporated under vacuum twice with Et_2O, to give the product as an orange amorphous powder (664 mg, yield: 98%). ^{1}H NMR ($CDCl_3$, 400 MHz): δ 10.13 (s, 1H), 8.26 (s, 1H), 7.42–7.40 (d, J = 9.01 Hz, 1H), 6.65–6.62 (m, 1H), 6.50–6.49 (d, J = 2.25 Hz, 1H), 3.50–3.45 (d, 4H), 1.28–1.24 (t, J = 14.26 Hz, 6H).

Synthesis of compound 3. This procedure is based on a literature report.[10] Sodium methanol (25% methanol, 7.6 mL, 33.6 mmol), 4-diethylaminobenzaldehyde (2 g, 13.6 mmol) and ((1,3-dioxolan-2-yl) methyl) triphenylphosphonium bromide (7.6 g, 17.6 mmol) were added to 80 ml of tetrahydrofuran, stirred at 78 °C for 12 hours, and the saturated ammonium chloride solution was added. At the end of the reaction, use dichloromethane extract reactants, the organic layer was dried by anhydrous sodium sulfate, and concentrated under reduced pressure. The crude product was added to 40 ml of tetrahydrofuran solution, then added hydrochloric acid, stirred at room temperature for 1 hour, neutralized with sodium hydroxide solution (2 M), extracted by dichloromethane, the organic layer was dried by anhydrous sodium sulfate, and distilled under vacuum and purified by column (petroleum ether/dichloromethane = 5:1, v/v) to obtain solid compound **3** (183 mg, yield: 35%). ^{1}H NMR ($CDCl_3$, 400 MHz): δ 9.72–9.59 (m, 1H), 7.73–7.71 (d, J = 8.63 Hz, 1H), 7.47–7.44 (d, J = 8.50 Hz, 1H), 7.39–7.36 (d, J = 15.63 Hz, 1H), 6.70–6.68 (d, J = 8.63 Hz, 2H), 6.57–6.53 (m, 1H), 3.48–3.41 (m, 4H), 1.27–1.20 (m, 6H).

Synthesis of compound 4. This procedure is based on a literature report.[10] Compound **1** (500 mg, 1.84 mmol), 4-diethylaminobenzaldehyde (2 g, 13.6 mmol) and ((1,3-dioxolan-2-yl) methyl) triphenylphosphonium bromide (7.6 g, 17.6 mmol) were added to 80 ml of tetrahydrofuran, stirred at 78 °C for 12 hours, and the saturated ammonium chloride solution was added. At the end of the reaction, use dichloromethane extract reactants, the organic layer was dried by anhydrous sodium sulfate, and concentrated under reduced pressure. The crude product was added to 40 ml of tetrahydrofuran solution, then added hydrochloric acid, stirred at room temperature for 1 hour, neutralized with sodium hydroxide solution (2 M), extracted by dichloromethane, the organic layer was dried by anhydrous sodium sulfate, and distilled under vacuum to obtain compound **4** (251 mg, yield: 48%). ^{1}H NMR ($CDCl_3$, 400 MHz): δ 9.66–9.64 (d, J = 7.63 Hz, 1H), 7.84 (s, 1H), 7.47–7.44 (d, J = 15.76 Hz, 1H), 7.37–7.34 (d, J = 8.88 Hz, 1H), 7.04–6.98 (m, 1H), 6.69–6.66 (d, J = 8.88 Hz, 1H), 6.53 (s, 1H), 3.50–3.44 (m, 4H), 1.27–1.24 (t, J = 14.26 Hz, 6H).

Synthesis of C-1. The compound was prepared according to a literature method.[4] Under N_2 atmosphere, a mixture of 1-ethyl-3,3'-dimethylindolium iodide (350 mg, 1.12 mmol) and 7-diethylamino-3-formylcoumarin (200 mg, 0.87 mmol) in absolute ethanol and catalytic amount of piperidine (0.4 mL). The reaction mixture was stirred under reflux for 5 hours. Then the solvent of the mixture was evaporated under reduced pressure. The crude product was purified with column chromatography (dichloromethane/methanol = 50:1, v/v). The compound was obtained as a brown solid (322 mg, yield: 83%). ^{1}H NMR ($CDCl_3$, 400 MHz): δ 10.19 (s, 1H), 8.60 (m, 1H), 8.03 (m, 1H), 7.54–7.50 (m, 4H), 7.44 (m, 1H), 6.70 (m, 1H), 6.46 (s,

1H), 4.86 (m, 4H), 3.52 (m, 2H) 1.84 (s, 6H), 1.64–1.60 (m, 3H) , 1.30–1.26 (m, 6H). ESI HRMS(M^+) *m*/*z*. calcd: 415.2380; found: 415.2387.

Synthesis of C-2. The compound was prepared according to a literature method.[3] Under N_2 atmosphere, a mixture of compound **4** (350 mg, 1.3 mmol) and 1-ethyl-3,3'-dimethylindolium iodide (490 mg, 1.56 mmol) in absolute ethanol were stirred at 78 °C for 5 hours. The crude product was purified with column chromatography (dichloromethane/methanol = 50:1, v/v), the product was obtained as a brown crystalline solid (365 mg, yield: 49%). ^{1}H NMR (DMSO-d_6, 400 MHz): δ 8.38–8.32 (m, 1H), 8.19 (s, 1H), 7.86–7.83 (m, 2H), 7.76 (m, 1H), 7.68 (m, 1H), 7.62–7.54 (m, 3H), 7.24 (m, 1H), 6.85–6.83(m, 1H), 6.62 (s, 1H), 4.54–4.49 (m, 2H), 3.55–3.49 (m, 4H), 1.74 (m, 6H), 1.43–1.39 (m, 3H), 1.18–1.15 (m, 6H); ^{13}C NMR ($CDCl_3$, 125 MHz): δ 180.43, 159.92, 157.11, 156.84, 152.95, 146.15, 143.97, 141.05, 131.79, 131.52, 129.25, 129.15, 123.51, 114.90, 114.54, 114.36, 110.86, 109.45, 96.79, 51.99, 45.01, 40.63, 40.42, 40.21, 39.59, 39.38, 31.43, 26.22, 14.44, 13.80, 12.90; ESI HRMS(M^+) *m*/*z*. calcd: 441.2537; found: 441.2548.

Synthesis of C-3. The compound was prepared according to a literature method.[3] Under N_2 atmosphere, a mixture of 1-ethyl-3,3'-dimethylindolium iodide (280 mg, 0.89 mmol) and 3-[4-(diethylamino) phenyl]-2-propenal (150 mg, 0.74 mmol) in absolute ethanol were stirred at 78 °C for 5 hours. The crude product was purified with column chromatography (dichloromethane/methanol = 50:1, v/v), the product was obtained as brown solid (102 mg, yield: 28%). ^{1}H NMR (DMSO-d_6, 400 MHz): δ 8.35–8.29 (m, 1H), 8.07 (m, 1H), 7.79–7.70 (m, 3H), 7.59–7.53 (m, 2H), 7.50–7.45 (m, 1H), 7.32–7.20 (m, 1H), 6.97 (m, 1H), 6.88 (m, 1H), 6.82 (m, 1H), 4.55–4.50 (m, 1H), 4.43–4.37 (m, 1H), 3.59–3.54 (m, 4H), 1.74 (m, 6H), 1.41–1.37 (m, 3H), 1.24–1.14 (m, 6H); ^{13}C NMR ($CDCl_3$, 125 MHz): δ 178.87, 157.28, 153.04, 151.31, 143.30, 141.22, 132.60, 129.37, 128.15, 123.88, 123.38, 122.97, 113.99, 113.49, 112.49, 110.60, 51.32, 44.66, 31.43, 26.67, 22.53, 14.44, 14.44, 13.03; ESI HRMS(M^+) *m*/*z*. calcd: 373.2638; found: 373.2642.

Synthesis of C-4. The compound was prepared according to a literature method.[2] Under N_2 atmosphere, a mixture of 3-ethyl-2-methylbenzothiazolium iodide (458 mg, 1.5 mmol), 4-diethylaminobenzaldehyde (266 mg, 1.5 mmol) and acetic anhydride (30 mL) was refluxed for 30 minutes. Then the reaction mixture was poured into a solution of potassium iodide (900 mg, 6 mmol) in warm water (30 mL). The precipitate was collected by filtration and dried in vacuum, the obtained solid product was washed with water (20 mL × 3), and recrystallized with ethanol. After drying, a black solid was obtained (560 mg, yield: 80%). ^{1}H NMR (DMSO-d_6, 400 MHz): δ 8.30 (m, 1H), 8.14–8.05 (m, 2H), 7.91 (m, 2H), 7.80–7.76 (m, 2H), 7.69–7.65 (m,

1H), 7.59 (m, 2H), 6.84 (m, 2H), 3.53 (m, 4H), 1.44–1.41 (m, 3H), 1.18–1.15 (m, 6H); ESI HRMS(M^+) *m/z*. calcd: 337.1733; found: 337.1737.

Synthesis of C-1-NB. The compound was prepared according to a literature method. The saturated solution of **C-1** (50 mg, 0.09 mmol) and **NB** (131.60 mg, 0.18 mmol) in methanol were prepared respectively, then the two different solution was mixed and stirred at room temperature for 1 hour. Afterward, deionized water (7 mL) was added dropwise, and the mixture was stirred for an hour. Bluish-gray precipitate was collected by filtration. After washing with methanol for several times, the product becomes pure, shown by TLC analysis. After drying in vacuum, the compound was obtained as a bluish-gray solid (39.0 mg), yield: 49%.^{1}H NMR (DMSO-d_6, 400 MHz): δ 8.80 (s, 1H), 8.29 (m, 1H), 7.86 (m, 3H), 7.58 (s, 3H), 7.02 (s, 3H), 6.92 (m, 7H), 6.72 (s, 1H), 4.48 (m, 2H), 3.57 (m, 4H), 3.32 (s, 3H), 2.17 (s, 9H), 1.71 (s, 6H), 1.46 (s, 3H), 1.17 (m, 10H), 0.87–0.72 (m, 6H); ^{13}C NMR ($CDCl_3$, 125 MHz): δ 180.75, 159.89, 158.15, 154.54, 150.79, 150.48, 143.82, 141.07, 132.90, 129.53, 129.08, 123.48, 114.82, 114.69, 112.69, 111.85, 109.95, 97.07, 55.39, 51.93, 45.35, 40.64, 40.43, 40.22, 40.01, 39.80, 39.59, 39.38, 26.58, 13.49, 12.97; ESI HRMS(M^+) *m/z*. calcd:415.2380; found:415.2383, ESI HRMS(M^-) *m/z*. calcd:471.1590; found:471.1592.

3. Molecular structure characterization data

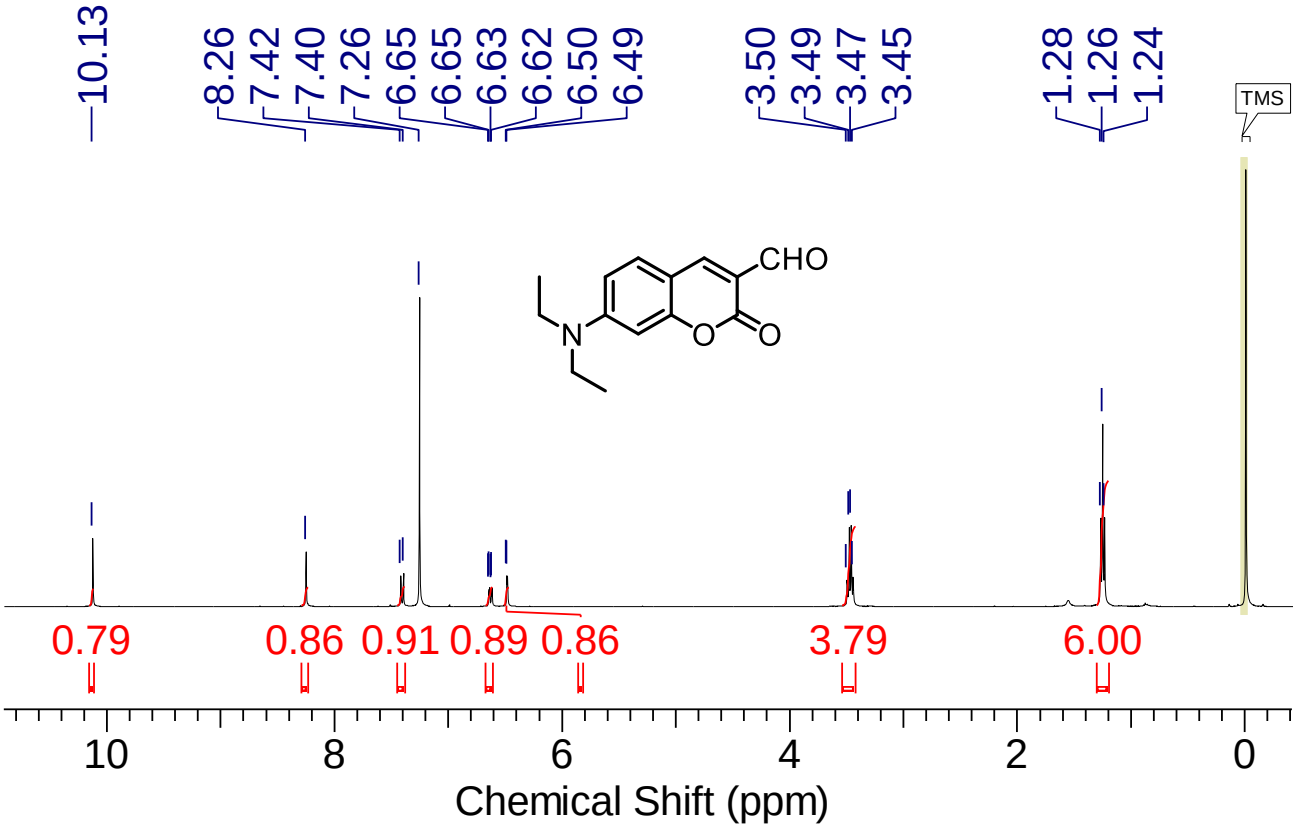

Figure S1. ^{1}H NMR spectrum of compound **1** (400 MHz, $CDCl_3$, ppm).

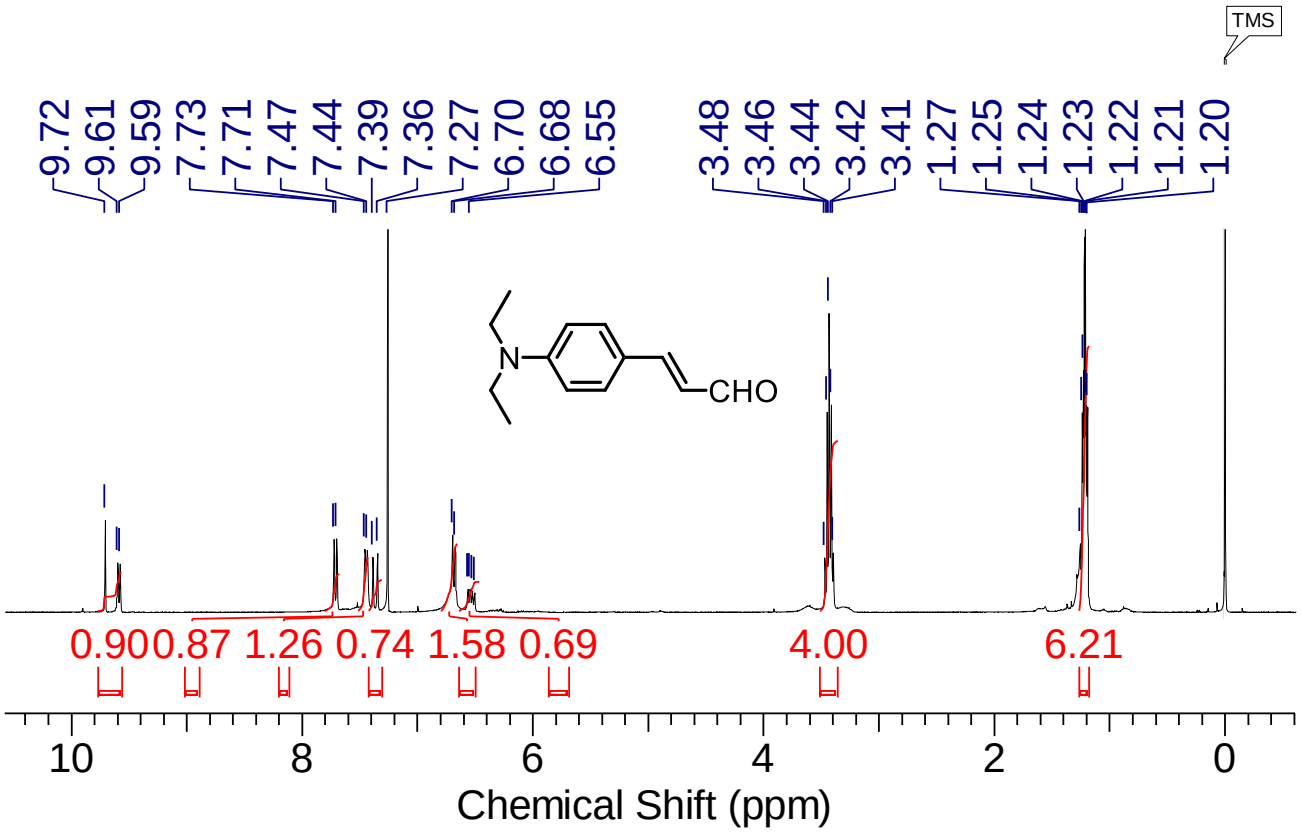

Figure S2. ^{1}H NMR spectrum of compound **3** (400 MHz, $CDCl_3$, ppm).

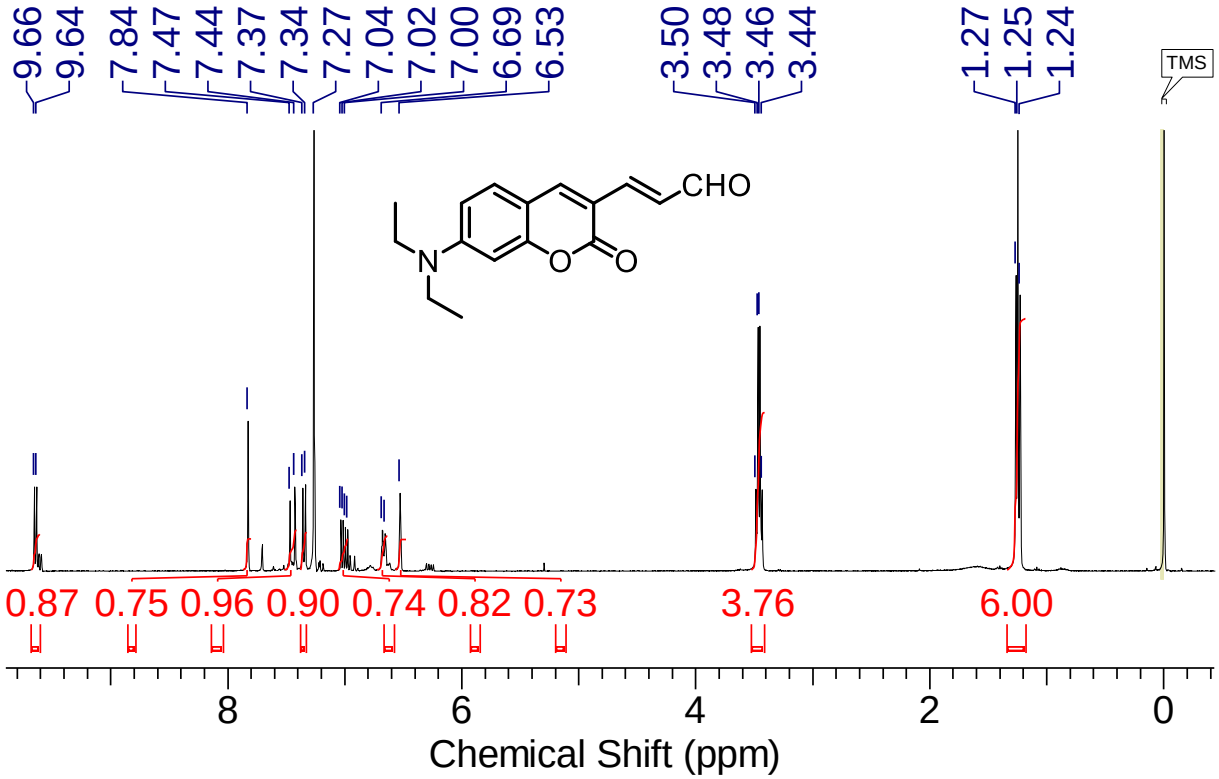

Figure S3. ^{1}H NMR spectrum of compound **4** (400 MHz, $CDCl_3$, ppm).

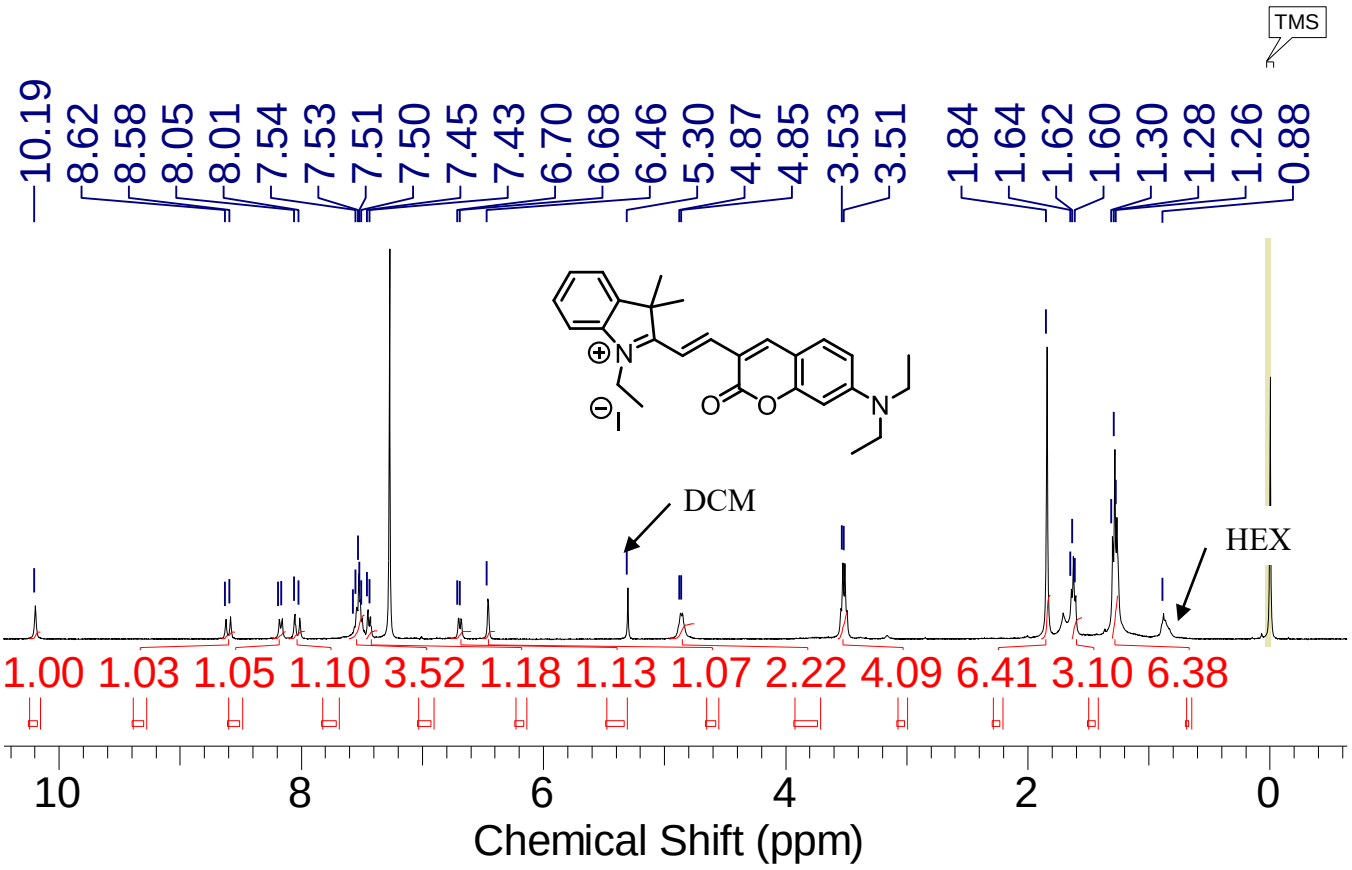

Figure S4. ^{1}H NMR spectrum of compound **C-1** (400 MHz, $CDCl_3$, ppm).

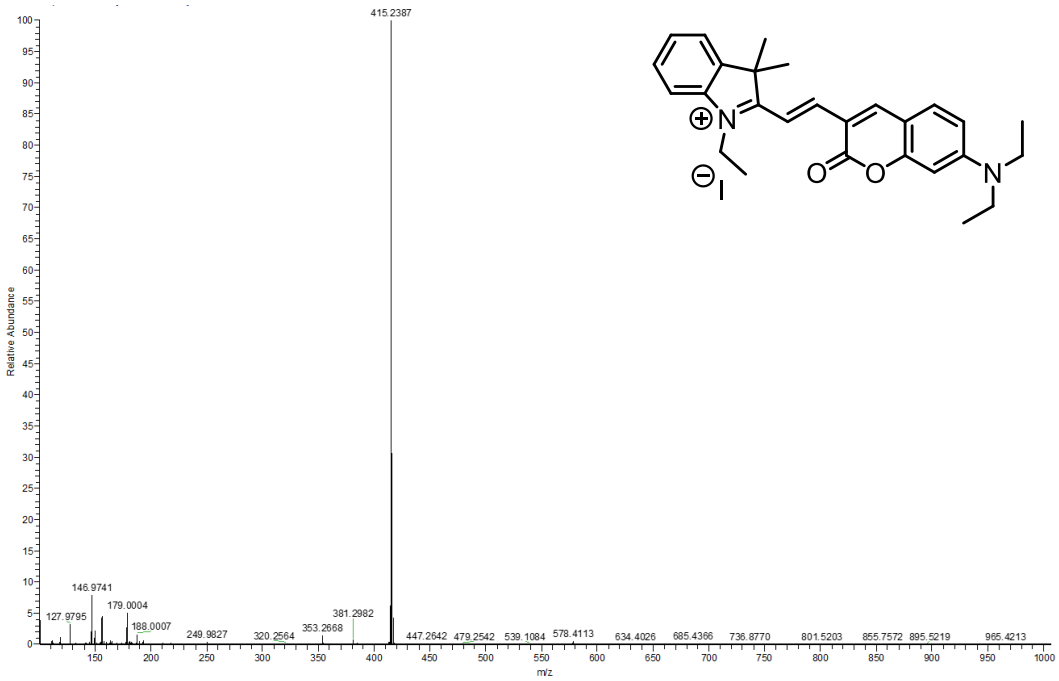

Figure S5. Ion trap ESI-HRMS of compound **C-1** (LTQ Orbitrap XL).

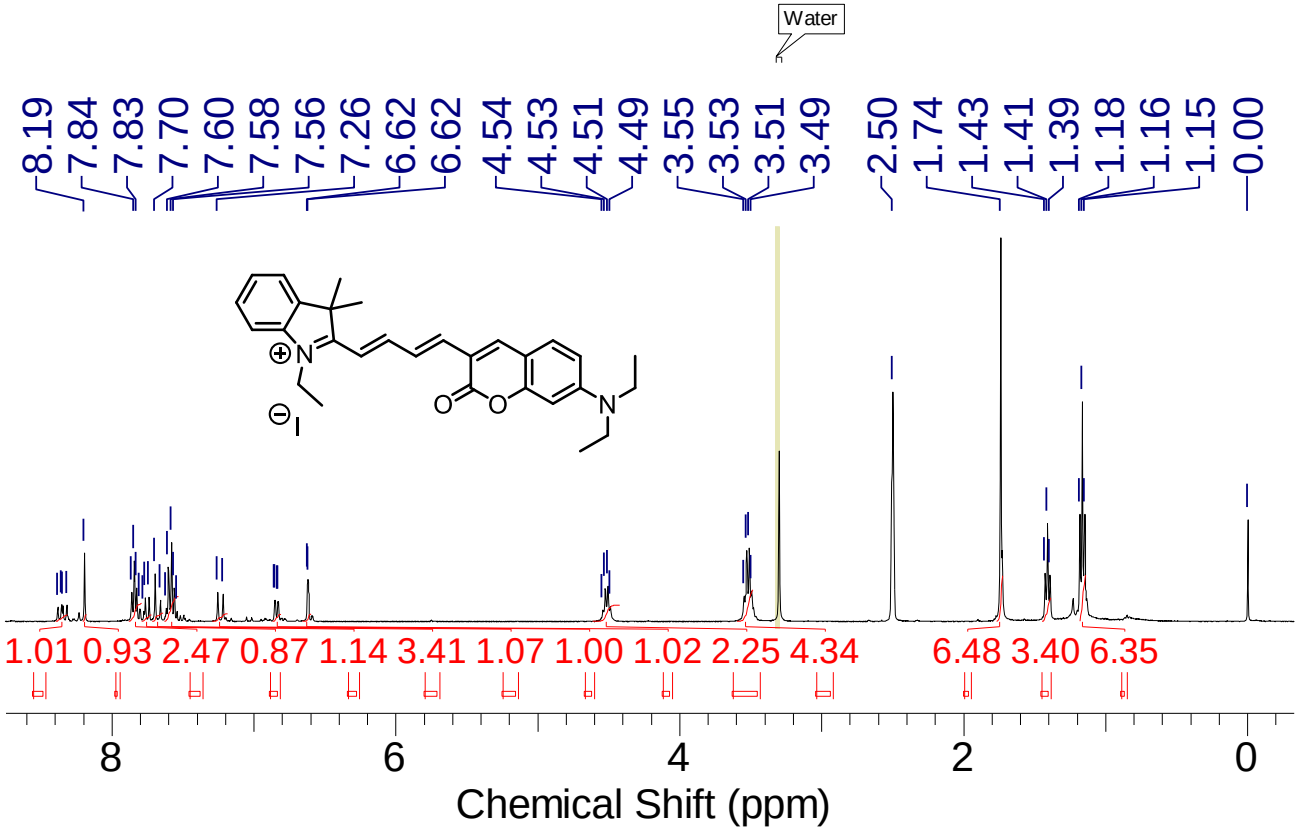

Figure S6. ^{1}H NMR spectrum of compound **C-2** (400 MHz, DMSO-d_6, ppm).

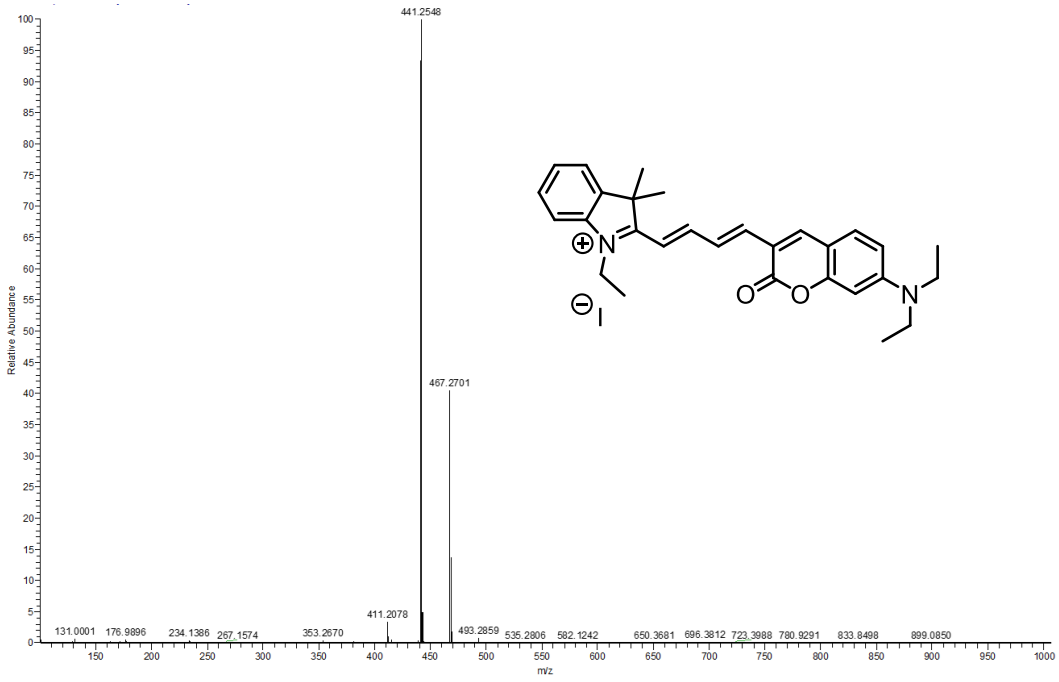

Figure S7. Ion trap ESI-HRMS of compound **C-2** (LTQ Orbitrap XL).

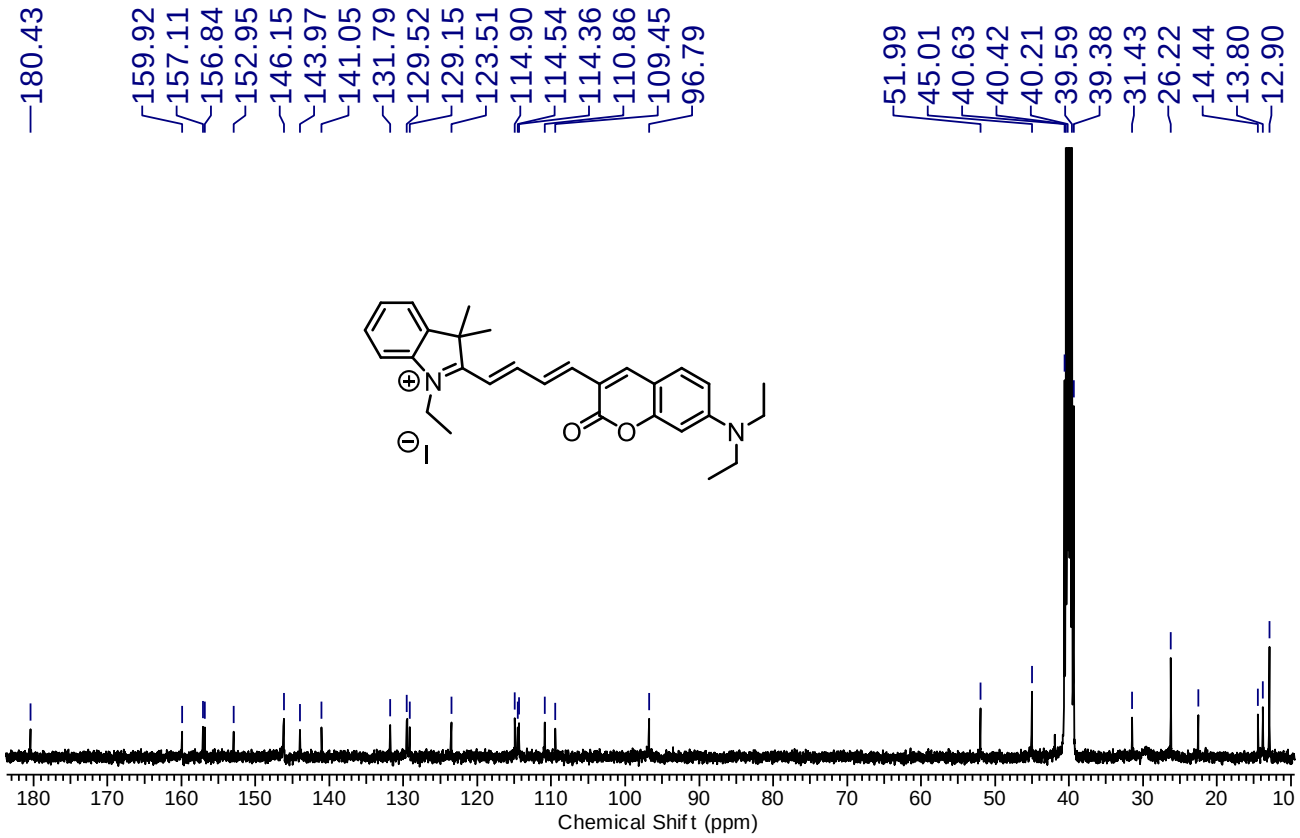

Figure S8. ^{13}C NMR spectrum of compound **C-2** (125 MHz, $CDCl_3$, ppm).

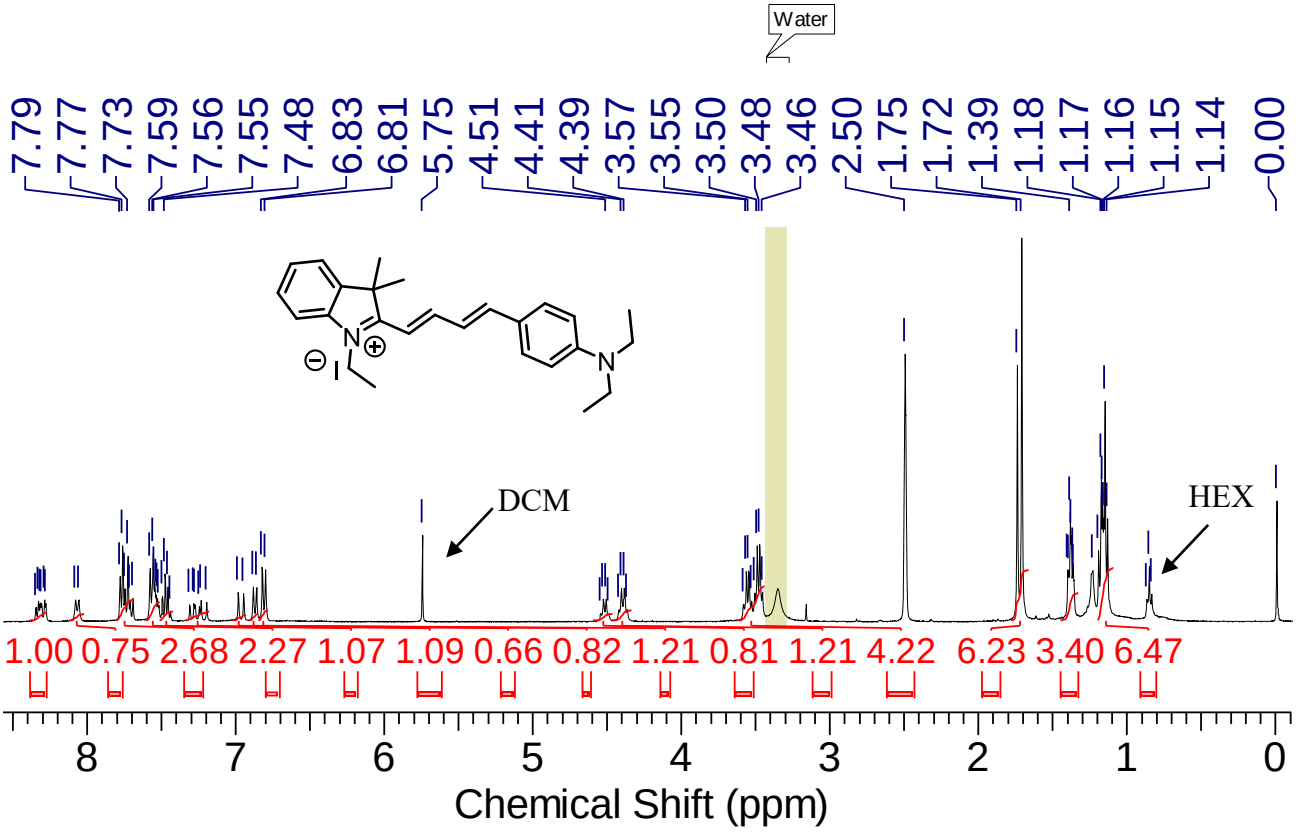

Figure S9. ^{1}H NMR spectrum of compound **C-3** (400 MHz, DMSO-d_6, ppm).

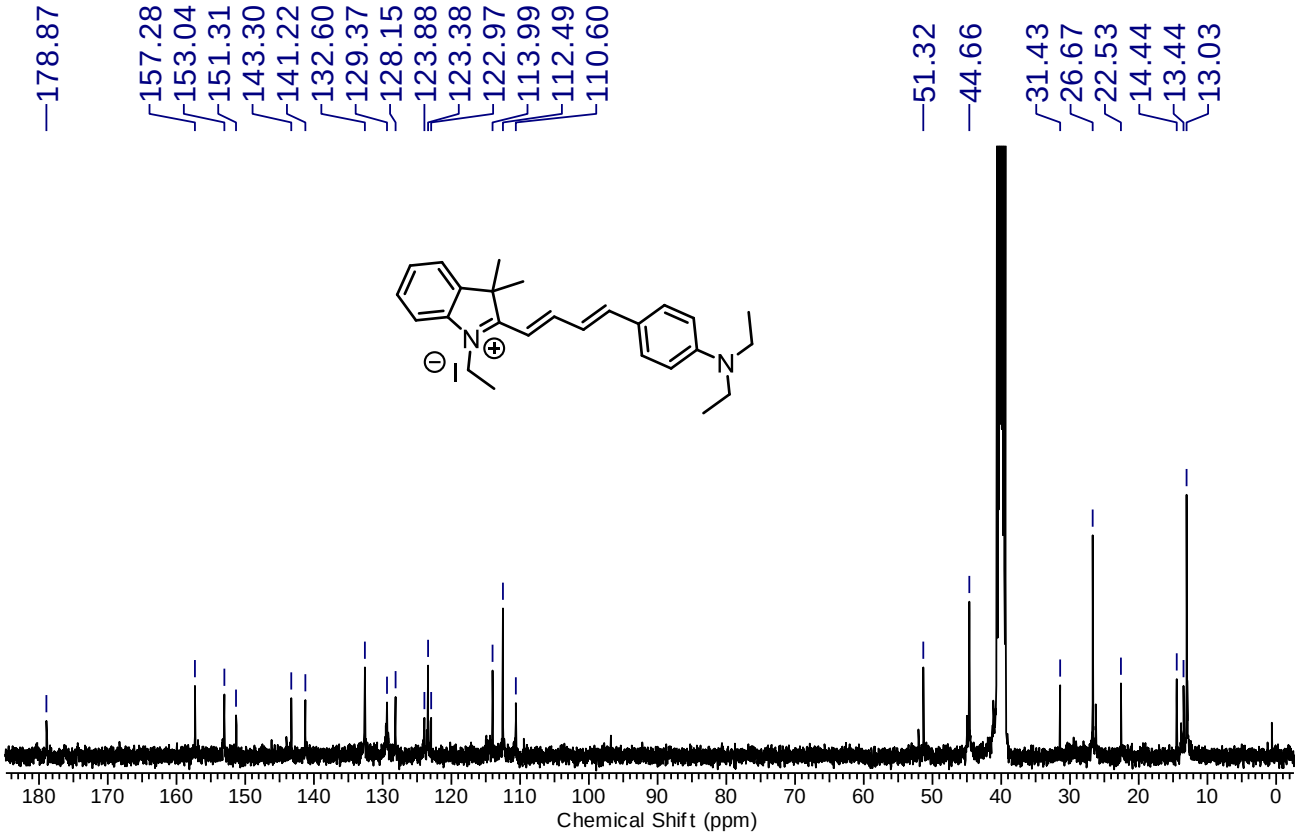

Figure S10. ^{13}C NMR spectrum of compound **C-3** (125 MHz, $CDCl_3$, ppm).

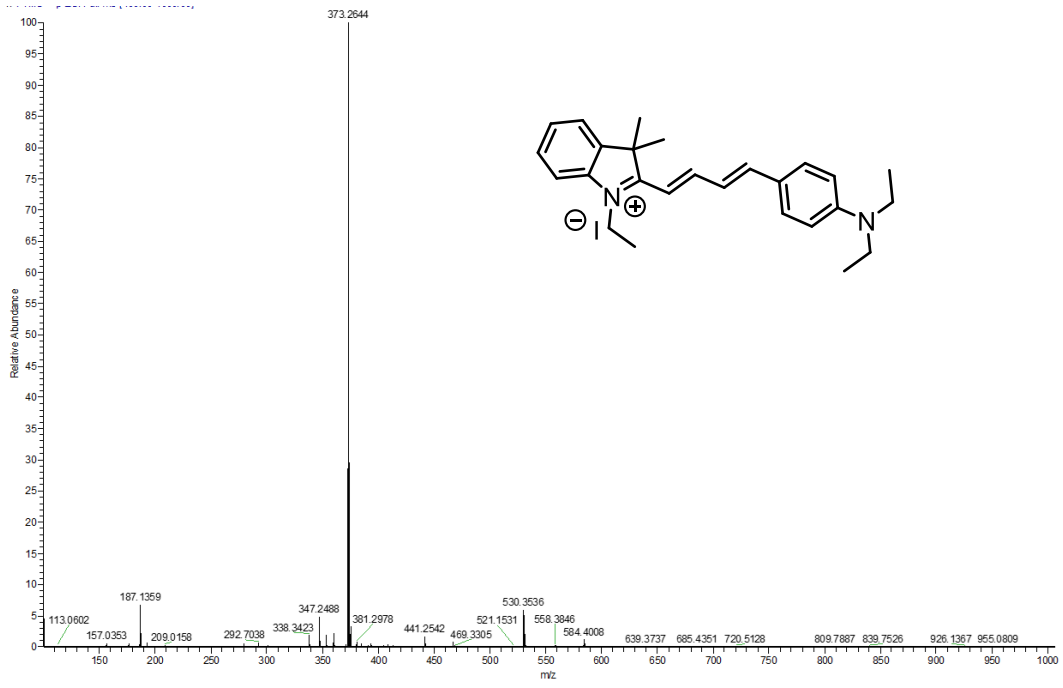

Figure S11. Ion trap ESI-HRMS of compound **C-3** (LTQ Orbitrap XL).

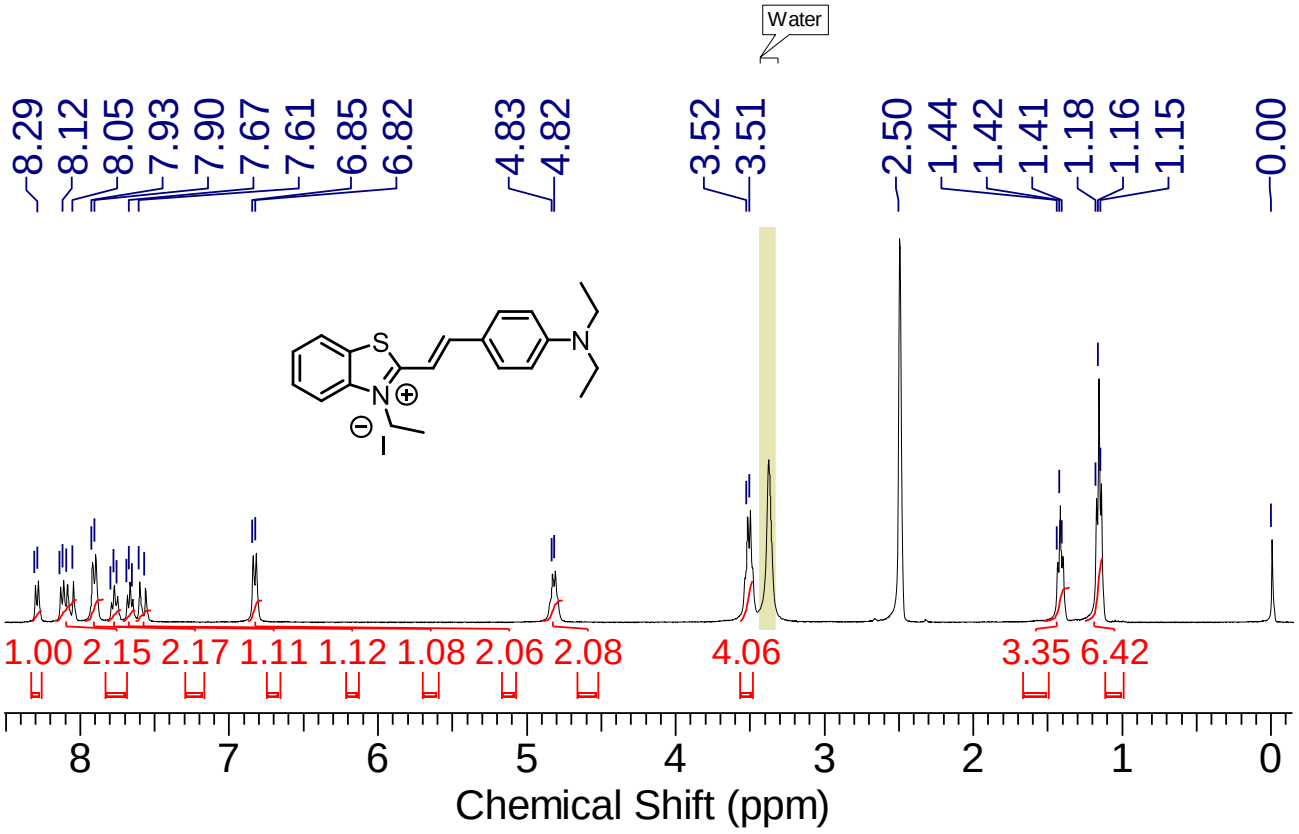

Figure S12. ^{1}H NMR spectrum of compound **C-4** (400 MHz, DMSO-d_6, ppm).

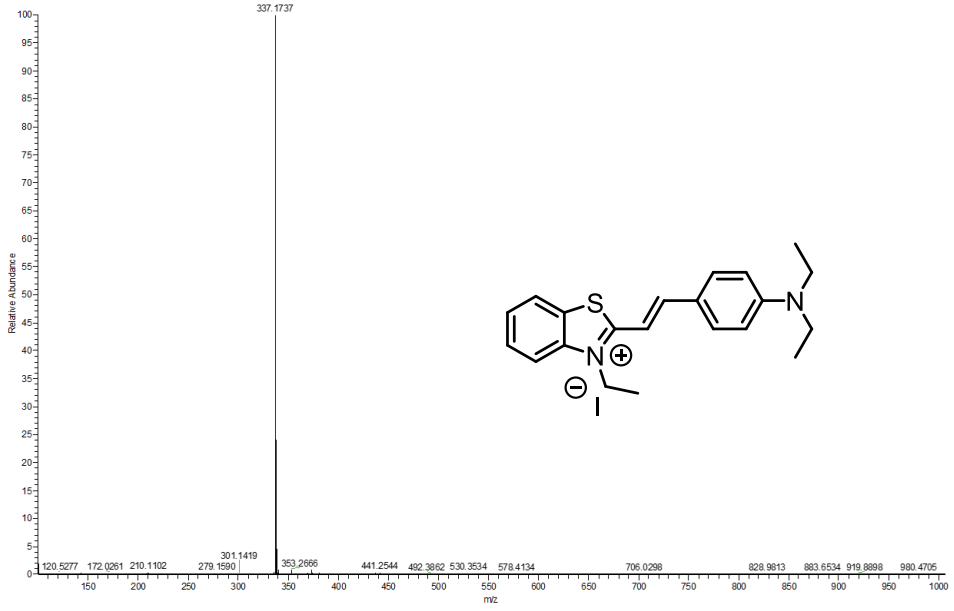

Figure S13. Ion trap ESI-HRMS of compound **C-4** (LTQ Orbitrap XL).

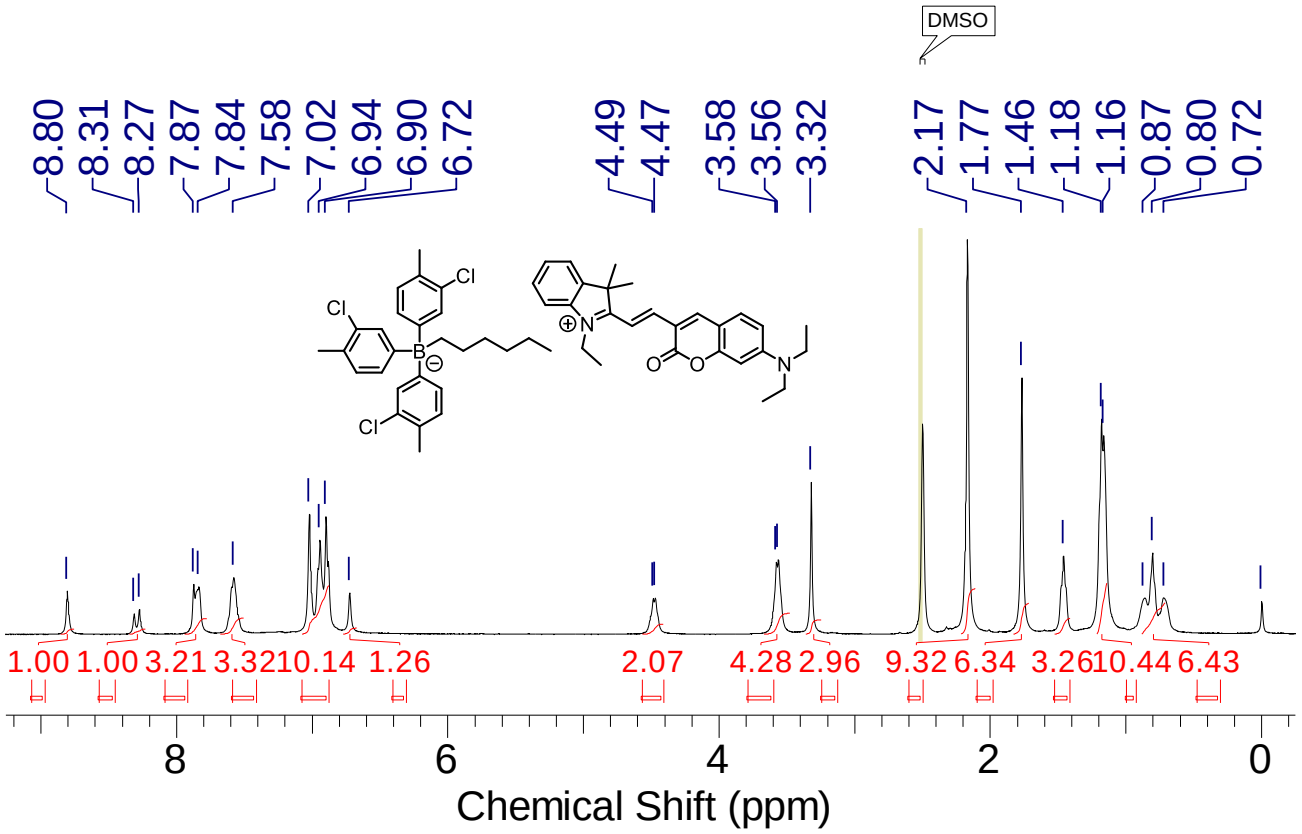

Figure S14. ^{1}H NMR spectrum of compound **C-1-NB** (400 MHz, DMSO-d_6, ppm).

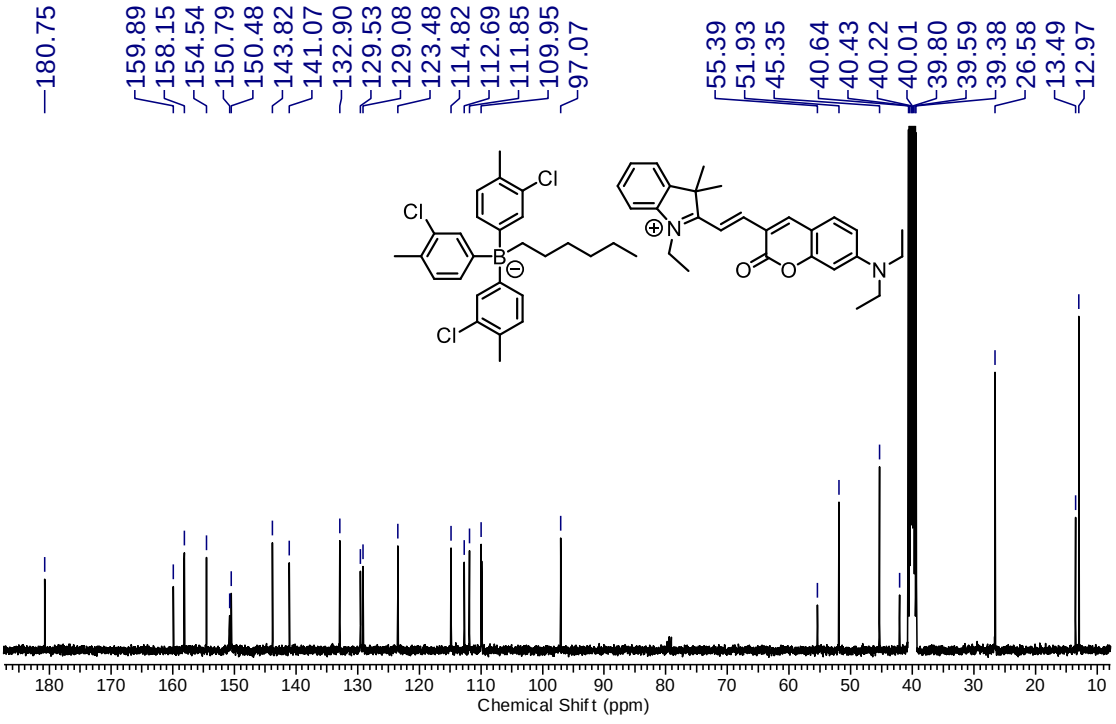

Figure S15. ^{13}C NMR spectrum of compound **C-1-NB** (125 MHz, $CDCl_3$, ppm).

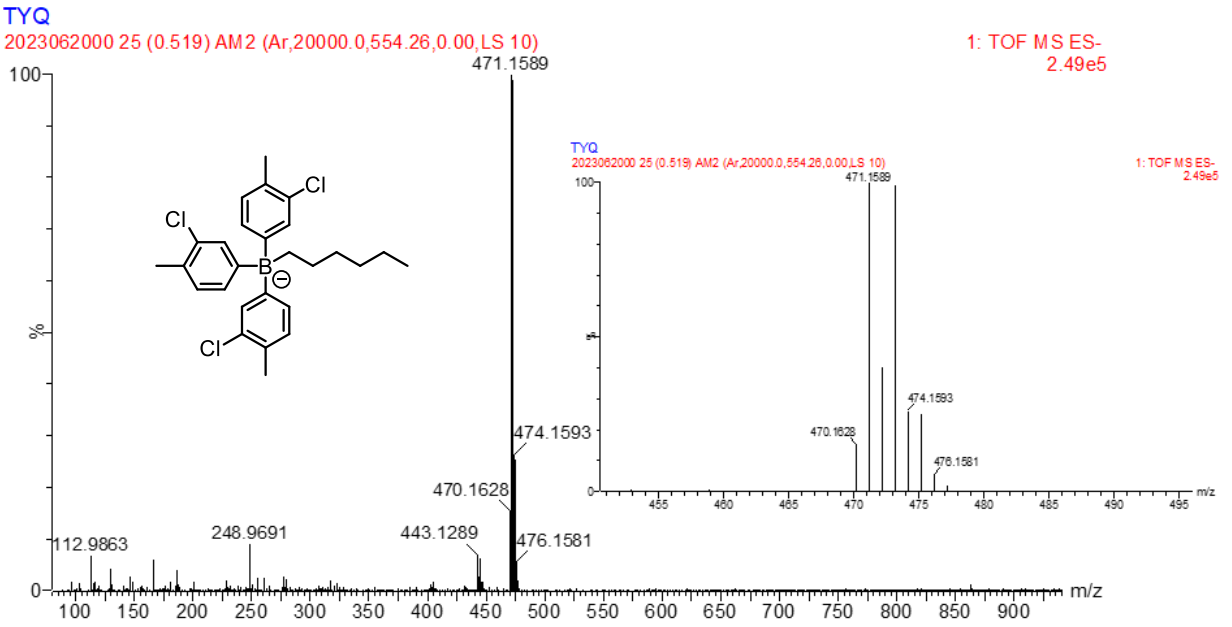

Figure S16. Ion trap ESI-HRMS of compound **C-1-NB** (anion) (LTQ Orbitrap XL).

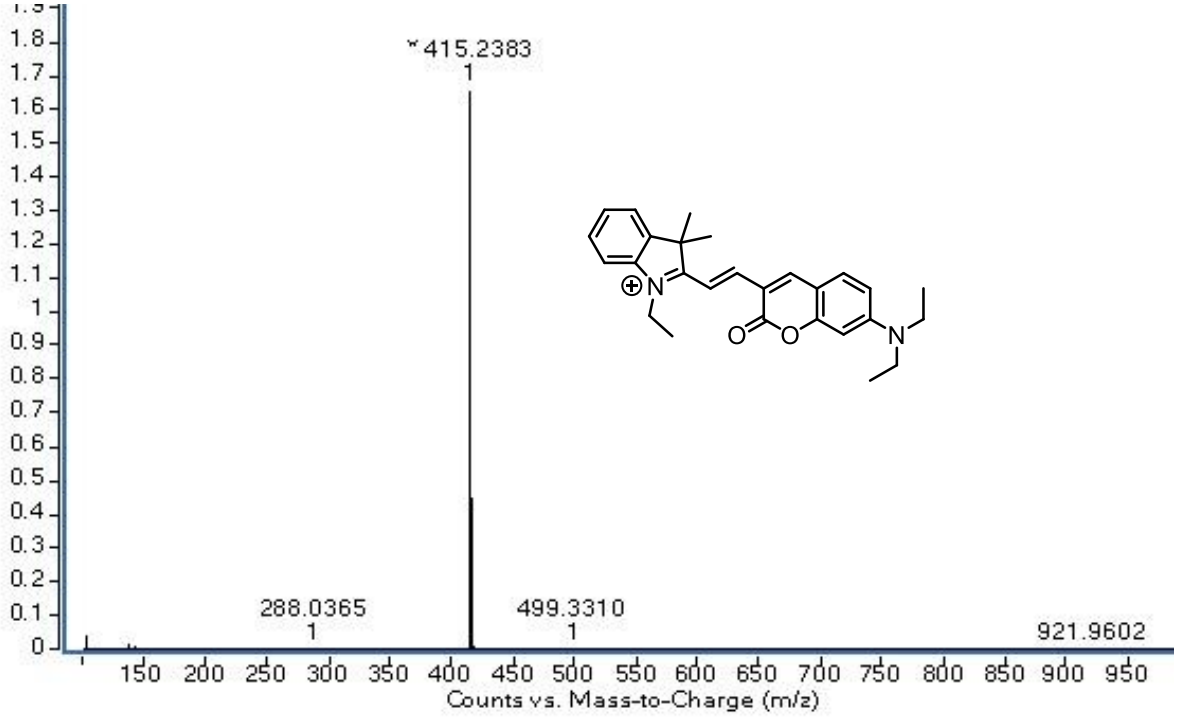

Figure S17. Ion trap ESI-HRMS of compound **C-1-NB** (cation) (LTQ Orbitrap XL).

4. Theoretical calculations

Table S1. Electronic Excitation Energies (eV) and Corresponding Oscillator Strengths (*f*), Main Configurations, and CI Coefficients of the Low-Lying Electronic Excited States of **C-1**.[a]

Electronic transition [b]	Energy [c]	*f* [d]	CI [e]
$S_0 \rightarrow S_1$	1.76 eV/702 nm	0.1047	0.90386
$S_0 \rightarrow S_2$	2.58 eV/480 nm	0.0299	0.85795
$S_0 \rightarrow S_3$	2.79 eV/444 nm	0.1242	0.93604
$S_0 \rightarrow T_1$	1.06 eV/1169 nm	0.1421	0.77220
$S_0 \rightarrow T2$	1.21 eV/1028 nm	0.0042	0.86262
$S_0 \rightarrow T3$	1.29 eV/962 nm	0.0456	0.88491

[a] The electronic transitions were calculated by TDDFT//B3LYP/6-31G(d), based on the DFT//B3LYP/6-31G(d)-optimized ground state and excited geometries. [b] TDDFT//B3LYP/6-31G(d), based on the DFT//B3LYP/6-31G(d)-optimized ground state geometries. [c] Only the selected low-lying excited states are presented. [d] Oscillator strengths. [e] CI coefficients are in absolute values.

Table S2. Electronic Excitation Energies (eV) and Corresponding Oscillator Strengths (f), Main Configurations, and CI Coefficients of the Low-Lying Electronic Excited States of **C-2**.[a]

Electronic transition [b]	Energy [c]	*f* [d]	CI [e]
$S_0 \rightarrow S_1$	1.69 eV/734 nm	0.0773	0.85073
$S_0 \rightarrow S_2$	2.41 eV/515 nm	1.2590	0.81305
$S_0 \rightarrow S_3$	2.68 eV/462 nm	0.1494	0.54585
$S_0 \rightarrow T_1$	0.99 eV/1255 nm	0.1671	0.83120
$S_0 \rightarrow T2$	1.38 eV/898 nm	0.0437	0.87090
$S_0 \rightarrow T3$	1.44 eV/863 nm	0.1197	0.86602

[a] The electronic transitions were calculated by TDDFT//B3LYP/6-31G(d), based on the DFT//B3LYP/6-31G(d)-optimized ground state and excited geometries. [b] TDDFT//B3LYP/6-31G(d), based on the DFT//B3LYP/6-31G(d)-optimized ground state geometries. [c] Only the selected low-lying excited states are presented. [d] Oscillator strengths. [e] CI coefficients are in absolute values.

Table S3. Electronic Excitation Energies (eV) and Corresponding Oscillator Strengths (f), Main Configurations, and CI Coefficients of the Low-Lying Electronic Excited States of **C-3**.[a]

Electronic transition [b]	Energy [c]	*f* [d]	CI [e]
$S_0 \rightarrow S_1$	2.10 eV/589 nm	0.0219	0.75513
$S_0 \rightarrow S_2$	2.76 eV/449 nm	0.2662	0.65911
$S_0 \rightarrow S_3$	2.88 eV/430 nm	1.0545	0.63262
$S_0 \rightarrow T_1$	0.64 eV/1923 nm	0.0006	0.67499
$S_0 \rightarrow T2$	0.81 eV/1532 nm	0.0006	0.78837
$S_0 \rightarrow T3$	0.96 eV/1287 nm	0.0364	0.64982

[a] The electronic transitions were calculated by TDDFT//B3LYP/6-31G(d), based on the DFT//B3LYP/6-31G(d)-optimized ground state and excited geometries. [b] TDDFT//B3LYP/6-31G(d), based on the DFT//B3LYP/6-31G(d)-optimized ground state geometries. [c] Only the selected low-lying excited states are presented. [d] Oscillator strengths. [e] CI coefficients are in absolute values.

Table S4. Electronic Excitation Energies (eV) and Corresponding Oscillator Strengths (f), Main Configurations, and CI Coefficients of the Low-Lying Electronic Excited States of **C-4**.[a]

Electronic transition [b]	Energy [c]	*f* [d]	CI [e]
$S_0 \rightarrow S_1$	2.37 eV/523 nm	0.0012	0.67626
$S_0 \rightarrow S_2$	2.44 eV/508 nm	0.0350	0.83020
$S_0 \rightarrow S_3$	2.72 eV/456 nm	0.0035	0.97624

[a] The electronic transitions were calculated by TDDFT//B3LYP/6-31G(d), based on the DFT//B3LYP/6-31G(d)-optimized ground state and excited geometries. [b] TDDFT//B3LYP/6-31G(d), based on the DFT//B3LYP/6-31G(d)-optimized ground state geometries. [c] Only the selected low lying excited states are presented. [d] Oscillator strengths. [e] CI coefficients are in absolute values.

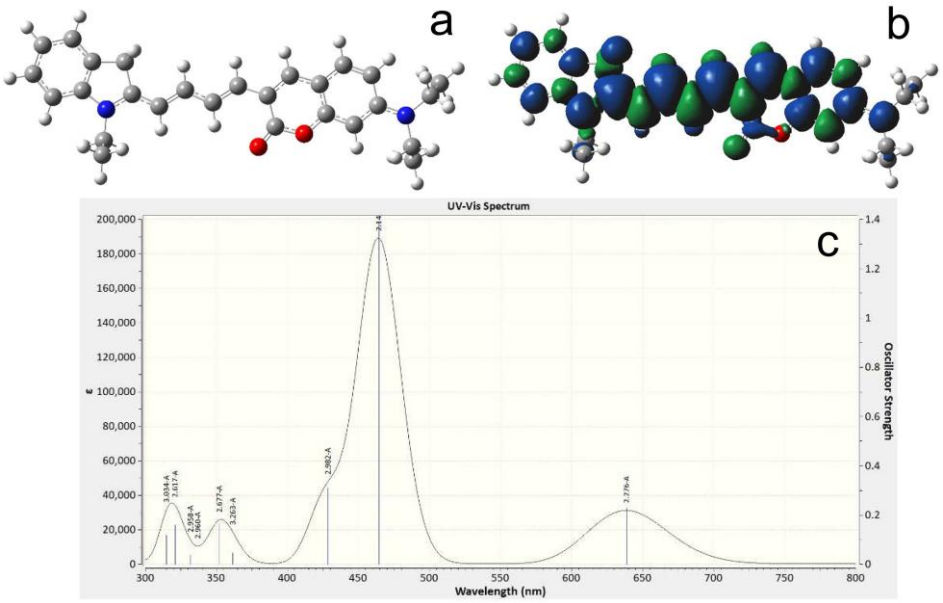

Figure S18. (a) The optimized ground state geometry of the reduced form of **C-1**. Calculated at UCAM-B3LYP/6-31G(d) level with Gaussian16, acetonitrile was used as solvent in the computation (CPCM model). A planar geometry was observed. (b) The electron spin density surface of the D_0 state of the reduced **C-1**. The α spin is shown in blue and β spin is shown in green. Calculated at UCAM-B3LYP/6-31G(d) level with Gaussian16, acetonitrile was used as solvent in the computation (CPCM model). (c) The calculated UV−Vis absorption spectra of the **C-1** radical. The main absorption band in the range of 400 – 500 nm is in good agreement with the nanosecond transient absorption spectrum shown in the main text of the manuscript.

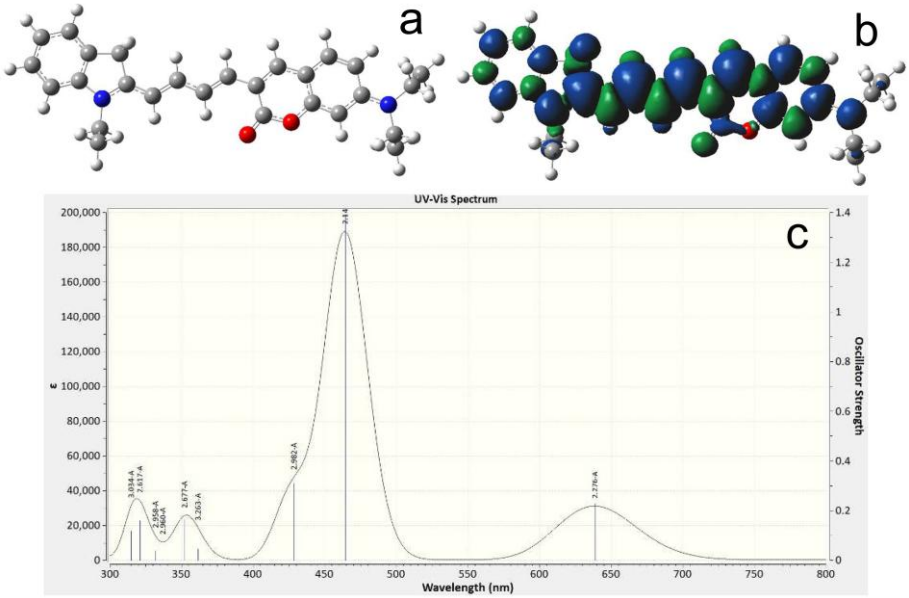

Figure S19. (a) The optimized ground state geometry of the reduced form of **C-2**. Calculated at UCAM-B3LYP/6-31G(d) level with Gaussian16, acetonitrile was used as solvent in the computation (CPCM model). A planar geometry was observed. (b) The electron spin density surface of the D_0 state of the reduced **C-2**. The α spin is shown in blue and β spin is shown in green. Calculated at UCAM-B3LYP/6-31G(d) level with Gaussian16, acetonitrile was used as solvent in the computation (CPCM model). (c) The calculated UV−Vis absorption spectra of the **C-2** radical.

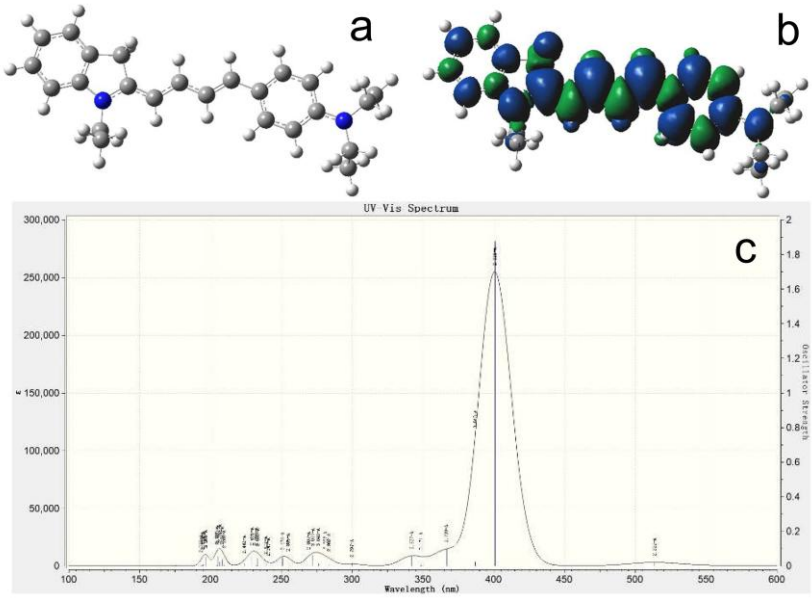

Figure S20. (a) The optimized ground state geometry of the reduced form of **C-3**. Calculated at UCAM-B3LYP/6-31G(d) level with Gaussian16, acetonitrile was used as solvent in the computation (CPCM model). A planar geometry was observed. (b) The electron spin density surface of the D_0 state of the reduced **C-3**. The α spin is shown in blue and β spin is shown in green. Calculated at UCAM-B3LYP/6-31G(d) level with Gaussian16, acetonitrile was used as solvent in the computation (CPCM model). (c) The calculated UV−Vis absorption spectra of the **C-3** radical.

5. UV–Vis absorption and fluorescence emission spectra

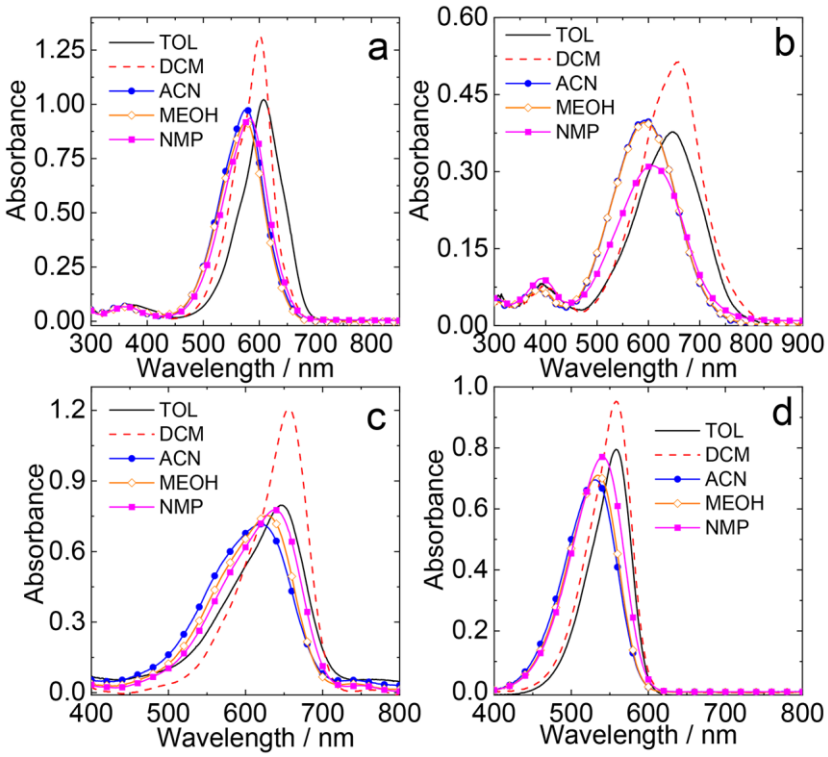

Figure S21. UV−vis absorption spectra of (a) **C-1**, (b) **C-2**, (c) **C-3** and (d) **C-4** in different solvents, c = 1.0 × 10^{-5} M, 25 °C.

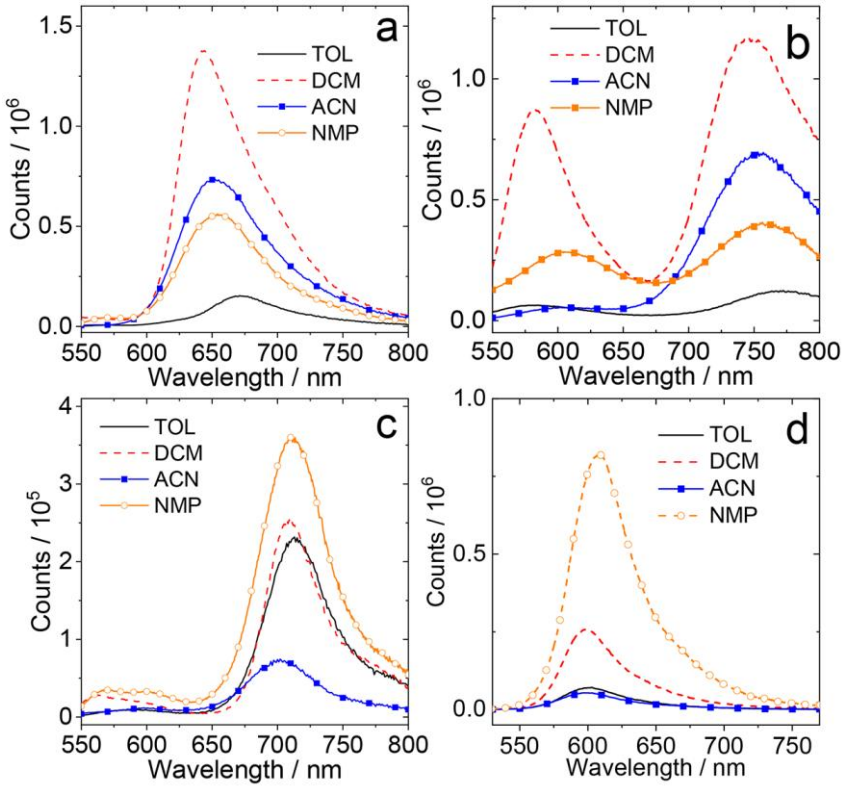

Figure S22. Fluorescence emission spectra of (a) **C-1**, (b) **C-2,** (c) **C-3** and (d) **C-4** in different solvents, λ_{ex} = 510 nm; A = 0.1, 25 °C.

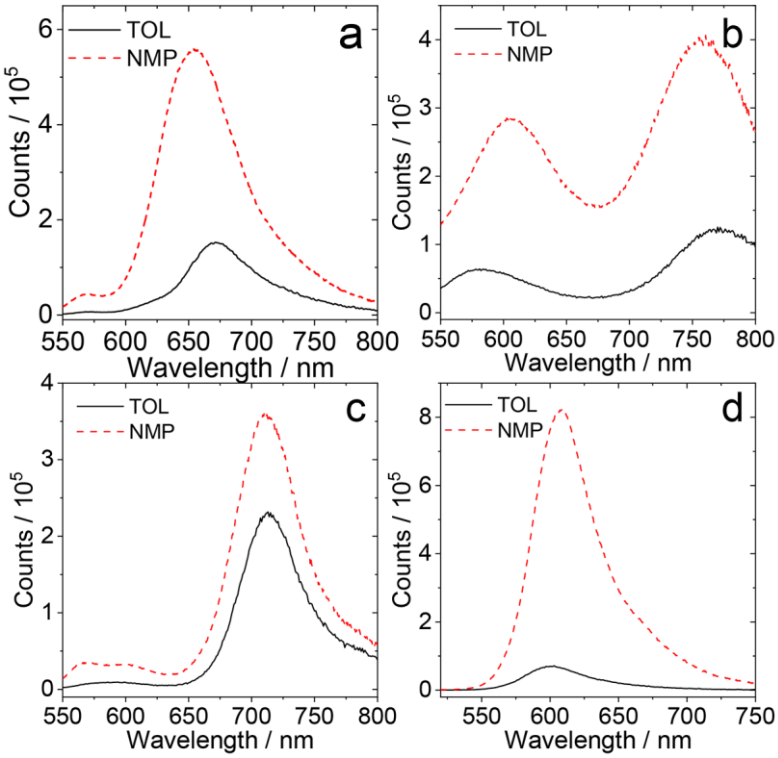

Figure S23. Comparation of fluorescence emission spectra of (a) **C-1**, (b) **C-2,** (c) **C-3** and (d) **C-4** in toluene (TOL) and 1-methyl-2-pyrrolidinone (NMP), λ_{ex} = 510 nm, A = 0.1, 25 °C.

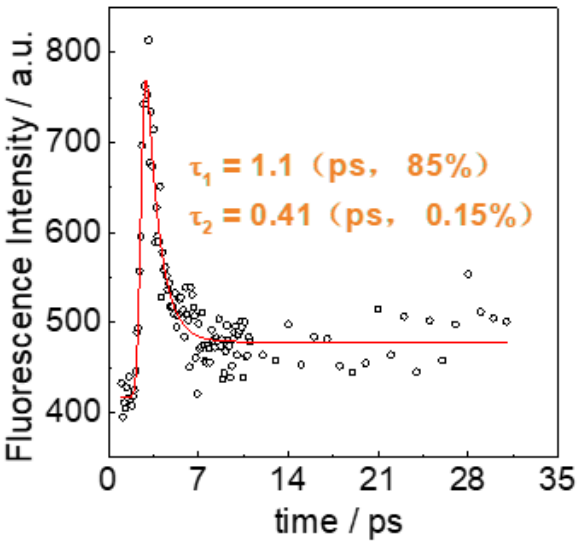

Figure S24. Fluorescence emission decay traces of **C-4**, λ_{ex} = 510 nm, c = 1.0 × 10 $^{-5}$ M in TOL, 25 °C.

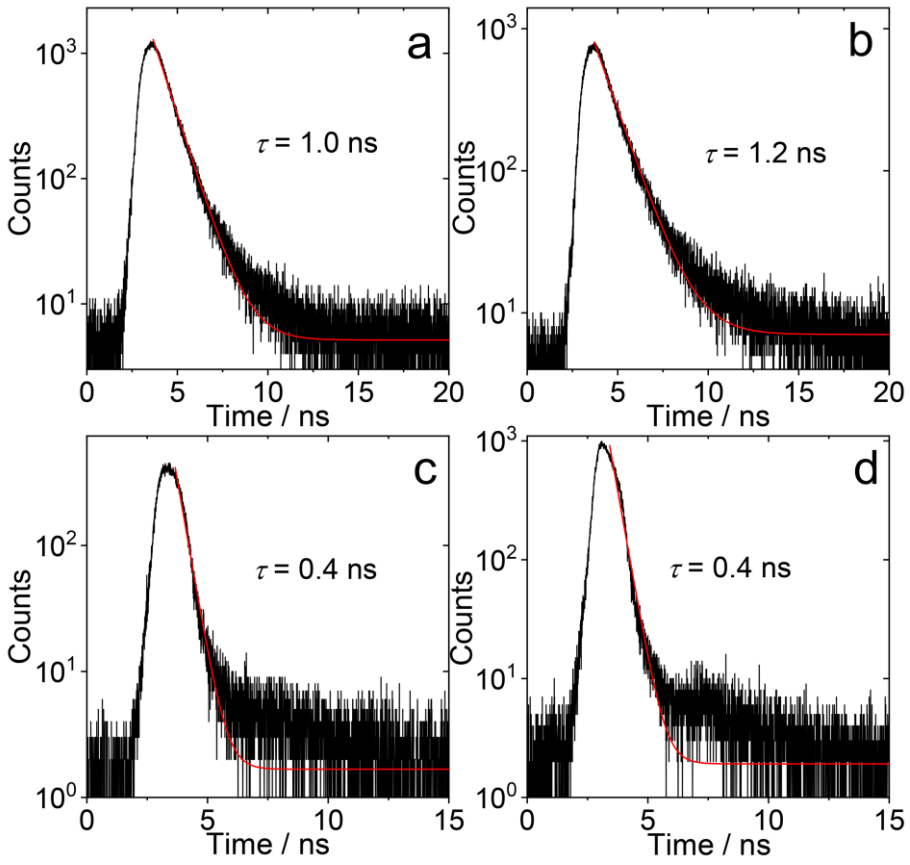

Figure S25. (a) Fluorescence emission decay traces of (a) **C-1**, λ_{em} = 650 nm. (b) **C-2**, λ_{em} = 750 nm. (c) **C-3**, λ_{em} = 710 nm. (d) **C-4**, λ_{em} = 610 nm, in NMP, λ_{ex} = 510 nm. c = 1.0 × 10^{-5} M, 25 °C.

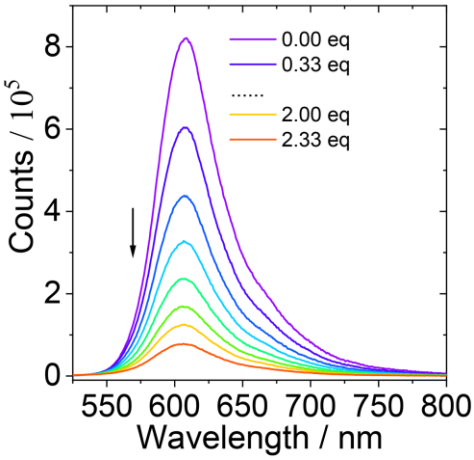

Figure S26. Fluorescence quenching of **C-4** upon incremental addition of NB, in 1-methyl-2-pyrrolidinone solution, λ_{ex} = 510 nm, c ≈ 1.0×10^{-5} M, 25 °C.

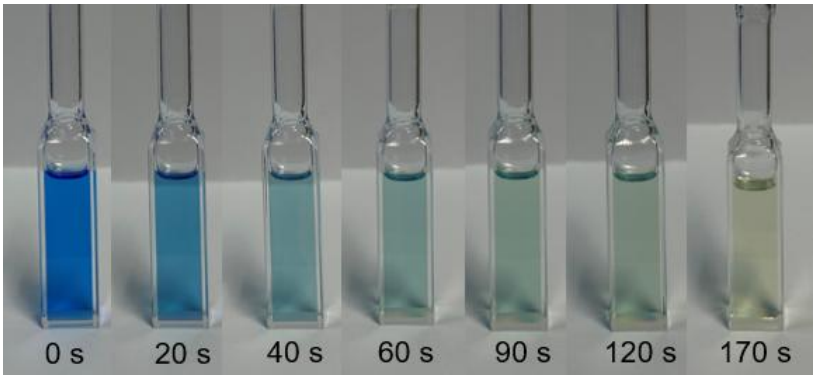

Figure S27. The variation of color of **C-4** and NB upon continuous photo-irradiation in deaerated TOL. Xenon lamp: 35 W (unfiltered white light intensity: 40 mW/cm^2), *c*[PSs] =3.3×10^{-5} M, *c*[NB] = 3.30×10^{-4} M, 25 °C.

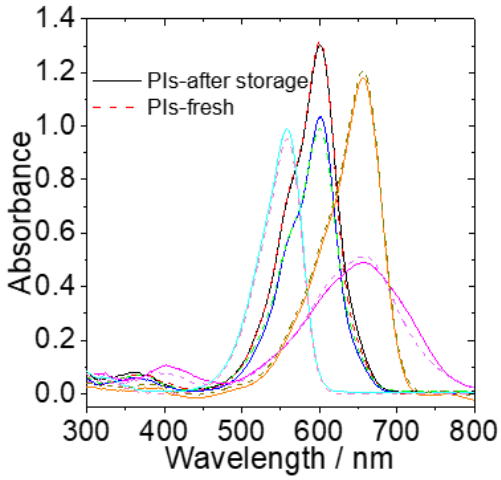

Figure S28. UV-Vis absorption spectra of the compounds (**C-1** ~ **C-4**, **C-1-NB**) before (fresh, dashed lines) and after (solid lines) storage under dark, dry, and room temperature (25 °C) conditions in DCM, *c* = 1.0×10^{-5} M, 25 °C.

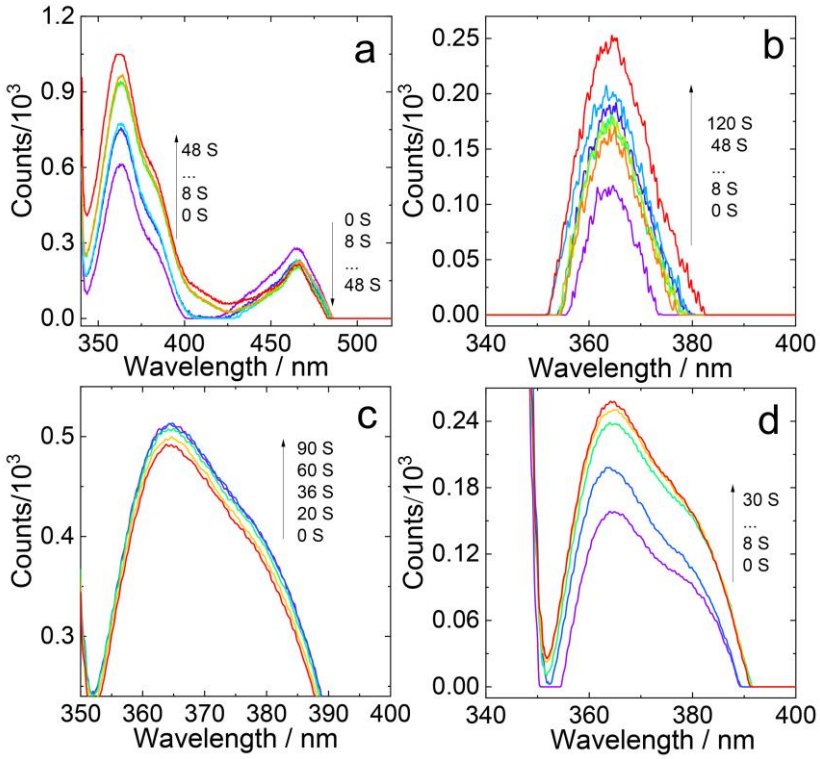

Figure S29. The change of fluorescence intensity of polymer during photopolymerization. (a) **C-1** and **NB**; (b) **C-2** and **NB**; (c) **C-3** and **NB**; (d) **C-4** and **NB**. Xenon lamp: 35 W (unfiltered white light intensity: 40 mW/cm^2), c[PSs] =3.3 ×10^{-5} M, c[NB] = 3.30 ×10^{-4} M, 25 °C.

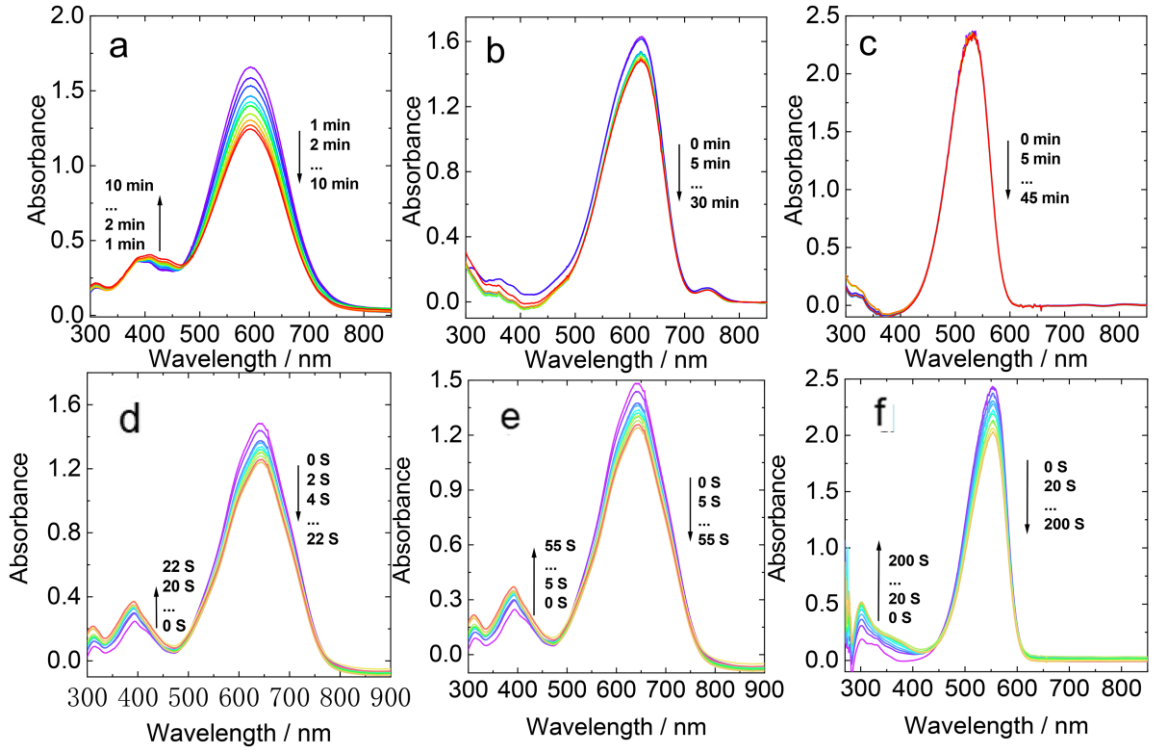

Figure S30. Photobleaching of the compounds in the presence of co-initiator **NB** upon white light irradiation, monitored by the evolution of the absorbance of compounds with irradiation time upon exposure to a 35 W xenon lamp (unfiltered white light intensity: 40 mW/cm^2) (a) **C-2** and **NB**, (b) **C-3** and **NB**, (c) **C-4** and **NB** in deaerated ACN; (d) **C-2** and **NB**, (e) **C-3** and **NB**, (f) **C-4** and **NB** in deaerated TOL, change of UV absorption curve with time of the compounds. c[PSs] =3.3 ×10^{-5} M, c[NB] = 3.30 ×10^{-4} M, 25 °C.

6. Femtosecond transient absorption spectra

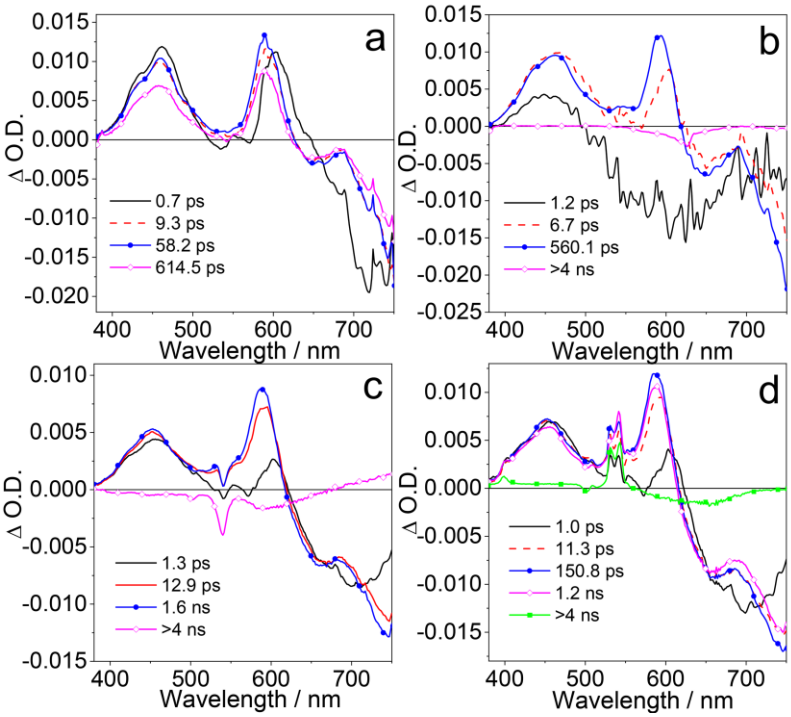

Figure S31. EADS obtained from global analysis of transient absorption data recorded for (a) **C-2** in ethyl-acetate (EtOAc), (b) **C-2** and NB mixed in situ with concentration ratio 1:1 in EtOAc, (c) **C-2** in ACN and (d) **C-2** and NB mixed in situ with concentration ratio 1:1 in ACN upon excitation at 540 nm.

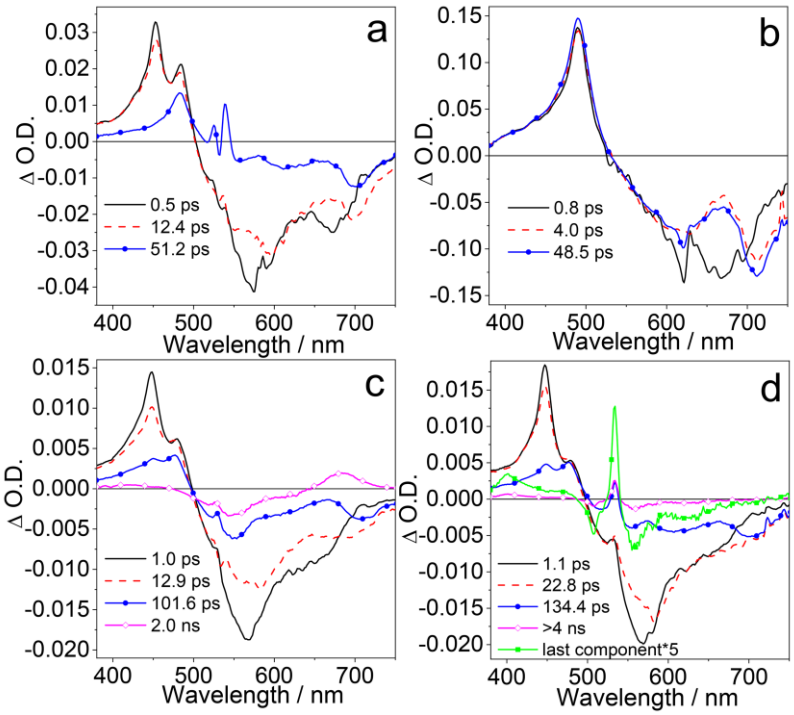

Figure S32. EADS obtained from global analysis of transient absorption data recorded for (a) **C-3** in EtOAc, (b) **C-3** and NB mixed in situ with concentration ratio 1:1 in EtOAc, (c) **C-3** in ACN and (d) **C-3** and NB mixed in situ with concentration ratio 1:1 in ACN upon excitation at 540 nm.

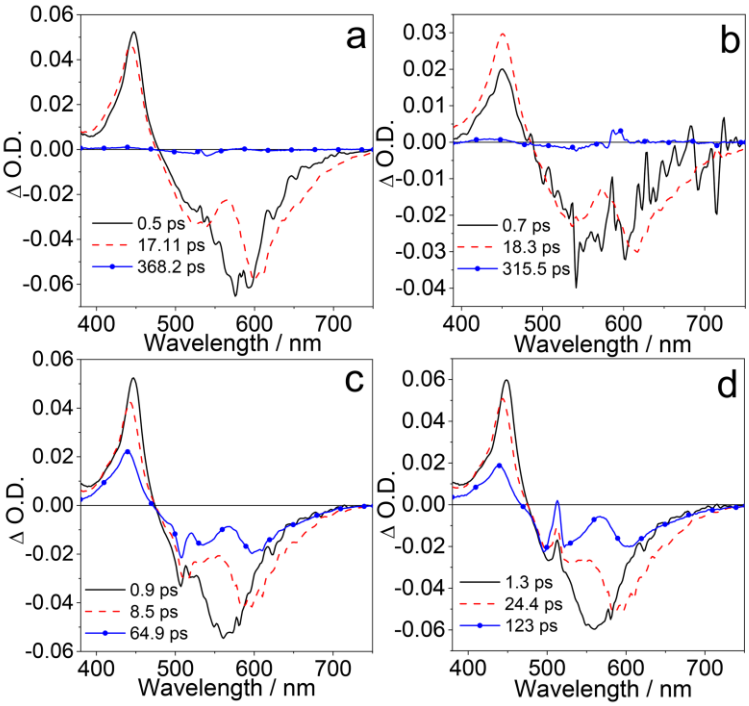

Figure S33. EADS obtained from global analysis of transient absorption data recorded for (a) **C-4** in EtOAc, (b) **C-4** and NB mixed in situ with concentration ratio 1:1 in EtOAc, (c) **C-4** in ACN and (d) **C-4** and NB mixed in situ with concentration ratio 1:1 in ACN upon excitation at 540 nm.

7. EPR spectra

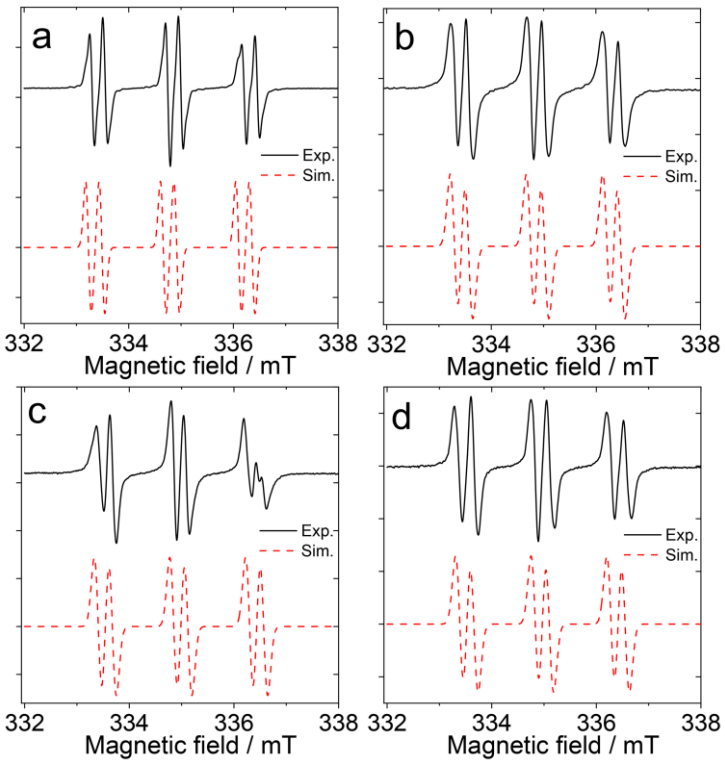

Figure S34. EPR spectra obtained from EPR-spin trapping experiments under irradiation of 35 W Xenon lamp (unfiltered white light intensity:40 mW/cm^2) using PBN for (a) **C-1**, (b) **C-2**, (c) **C-3** and (d) **C-4** in tert-Butylbenzene/anhydrous (v/v 5:1) detected at Xenon light at 25 °C (black solid lines). The dotted lines are the simulation spectra, c[PSs] = 2.0 × 10^{-4} M, c[NB] = 1.0 × 10^{-2} M, c[PBN] = 2.0 × 10^{-2} M.

8. Double bond conversions

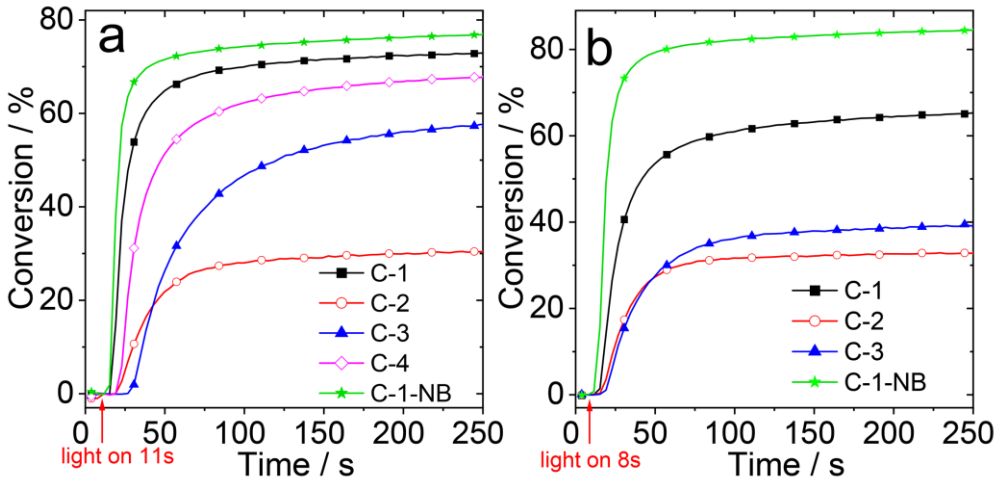

Figure S35. Photopolymerization profiles of TMPTA/TOL in the presence of **C-1**, **C-2**, **C-3**, **C-4**, **C-1-NB** and NB. PSs/NB (0.5 wt%/1.2 wt%). For **(a)**, the light source at 540 nm with 1.0 mW/cm^2 irradiation intensity; For **(b)**, the light source at 620 nm with 1.0 mW/cm^2 irradiation intensity density. Arrows indicate start of irradiation.

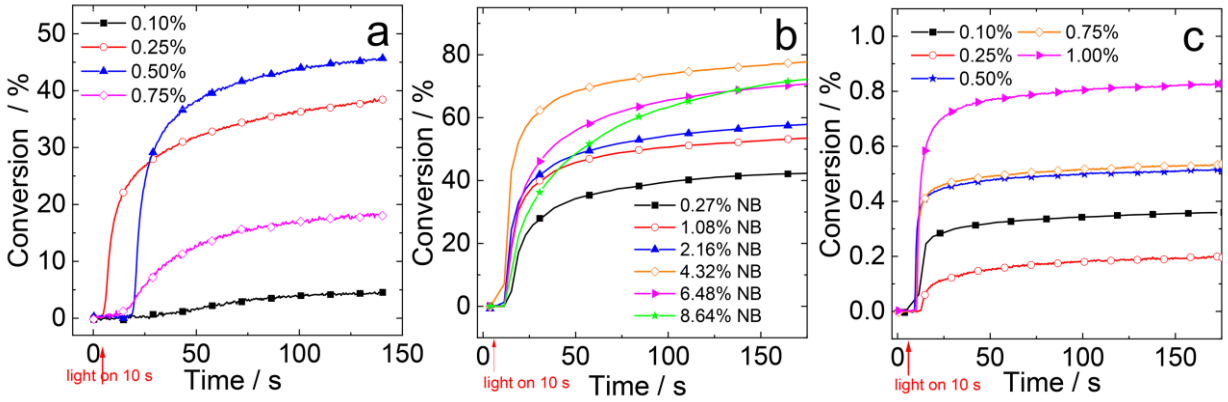

Figure S36. Relationship between the degree of double bond (–CH=CH–) conversion of TMPTA and irradiation time. (a) different concentration of **C-1** + 0.40% NB, (b) 1.09% **C-1** + different concentration of NB, (c) different concentration of **C-1-NB** + 0.40% NB, 25 °C.

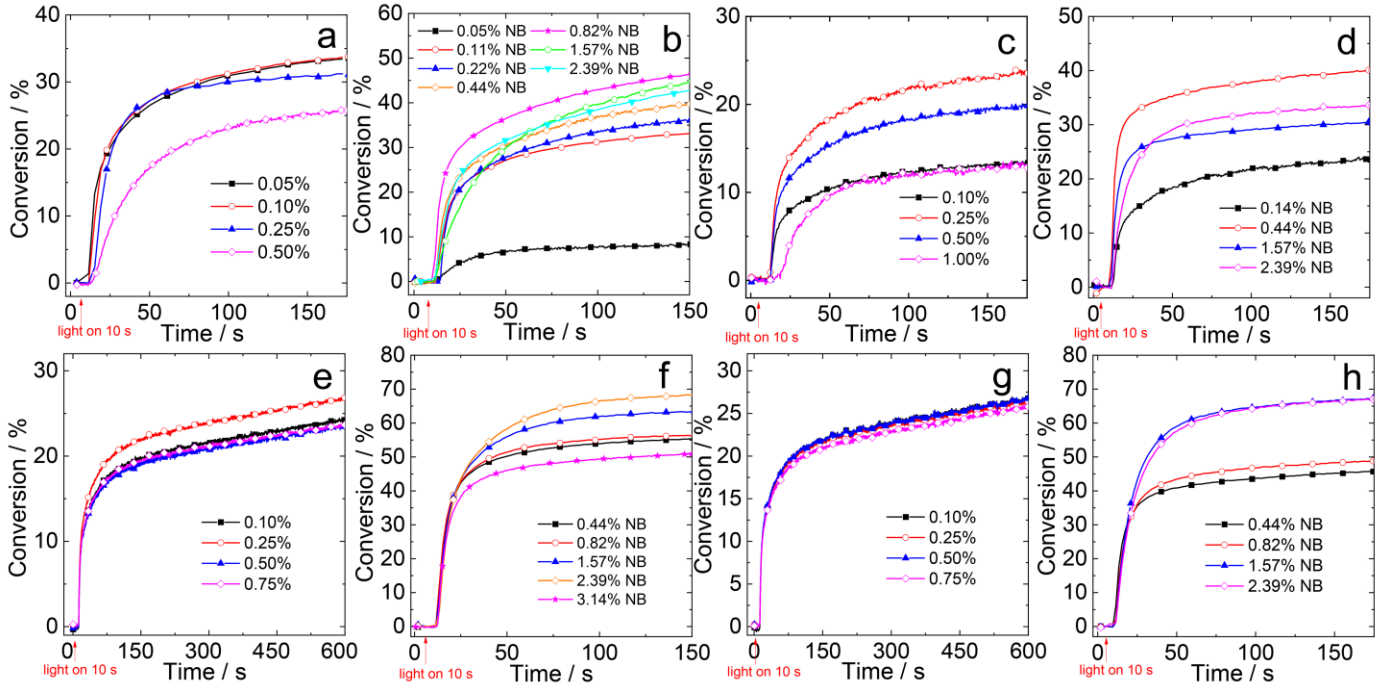

Figure S37. Relationship between the degree of double bond (–CH=CH–) conversion of TMPTA and irradiation time. (a) different concentration of **C-2** + 0.40% NB, (b) 0.22% **C-2** + different concentration of NB, (c) different concentration of **C-3** + 0.40% NB, (d) 0.55% **C-3** + different concentration of NB, (e) different concentration of **C-4** + 0.40% NB, (f) 1.63% **C-4** + different concentration of NB, (g) different concentration of **C-0** + 0.40% NB, (h) 1.63% **C-0** + different concentration of NB, 25 °C.

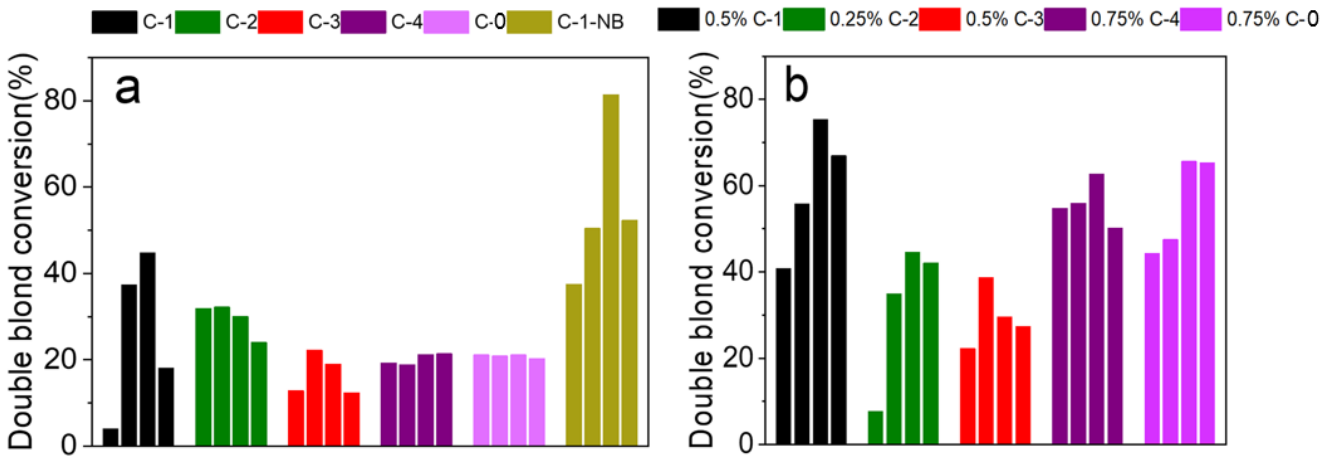

Figure S38. Relationship between the rates of double bond (–CH=CH–) conversion of TMPTA and different PSs/NB content in the blends, (a) from left to right for every photoinitiation: **C-1** (0.1%, 0.25%, 0.5%, 0.75%) + 0.4% NB, **C-2** (0.05%, 0.1%, 0.25%, 0.5%) + 0.4% NB, **C-3** (0.1%, 0.25%, 0.5%, 0.75%) + 0.4% NB, **C-4** (0.1%, 0.25%, 0.5%, 0.75%) + 0.4% NB, **C-0** (0.1%, 0.25%, 0.5%, 0.75%) + 0.4% NB, **C-1-NB** (0.25%, 0.5%, 0.75%,1.0%) + 0.4% NB on 120 s, (b) from left to right for every photoinitiation: 0.5% **C-1** + (0.27%, 2.16%, 4.32%, 8.64%) NB, 0.25% **C-2** + (0.05%, 0.22%, 0.82%, 2.39%) NB, 0.5% **C-3** + (0.14%, 0.44%, 1.57%, 2.39%) NB, 0.75% **C-4** + (0.44%, 0.82%, 1.57%, 3.14%) NB, 0.75% **C-0** + (0.44%, 0.82%,1.57%, 2.39%) NB on 120 s. (For **C-1**, **C-2**, **C-3**, **C-1-NB**: the following light-emitting diodes (LEDs) were used as irradiation sources: LED at 620 nm = incident light intensity at the sample surface: I_0 = 1.0 mW/cm^2; For **C-0**, **C-4**: LED at 540 nm, I_0=1.0 mW/cm^2), in TOL, 25 °C.

9. References

(1) Toba, Y.; Yasuike, M.; Usui, Y. The Onium Butyltriphenylborates as Novel Donor–Acceptor Initiators for Free Radical Photopolymerization. *Chem. Commun.* **1997**, 675−676.

(2) Je, J. T.; Lee, K. Y.; Min, K. S. Hemicyanine Dye for Optical Recording. *Mol. Cryst. Liq. Cryst.* **2001**, *371* (1), 223−226.

(3) Brockmann, S.; Arnold, T.; Schweder, B.; Bernhard, G. Visualizing Acidophilic Microorganisms in Biofilm Communities Using Acid Stable Fluorescence Dyes. *J. Fluoresc.* **2010**, *20* (4), 943−951.

(4) Johnson, R. E.; van der Zalm, J. M.; Chen, A.; Bell, I. J.; Van Raay, T. J.; Al-Abdul-Wahid, M. S.; Manderville, R. A. Unraveling the Chemosensing Mechanism by the 7-(Diethylamino)coumarin-Hemicyanine Hybrid: A Ratiometric Fluorescent Probe for Hydrogen Peroxide. *Anal. Chem.* **2022**, *94* (31), 11047−11054.

(5) Frisch, M. J.; Trucks, G. W.; Schlegel, H. B.; Scuseria, G. E.; Robb, M. A.; Cheeseman, J. R.; et al. Gaussian 16 rev. C.01; *Wallingford. CT*, **2016**.

(6) Neese, F. Software Update: The ORCA Program System—Version 6.0. *WIREs Comput. Mol. Sci.* **2025**, *15* (2), e70019.

(7) Snellenburg, J.; Laptenok, S.; Seger, R.; Mullen, K.; Van Stokkum, I. Glotaran: A Java-based Graphical User Interface for the R Package TIMP. *J. Stat. Softw.* **2012**, *49*, 1−22.

(8) Deng, L.; Tang, L.; Qu, J. Novel Chalcone-based Phenothiazine Derivative Photoinitiators for Visible Light Induced Photopolymerization with Photobleaching and Good Biocompatibility. *Prog. Org. Coat.* **2022**, *167*, 106859.

(9) Renault, K.; Renard, P. Y.; Sabot, C. Detection of Biothiols with a Fast-Responsive and Water-Soluble Pyrazolone-based Fluorogenic Probe. *Eur. J. Org. Chem.* **2018**, 6494−6498.

(10) Yuan, L.; Lin, W.; Yang, Y. A Ratiometric Fluorescent Probe for Specific Detection of Cysteine over Homocysteine and Glutathione Based on the Drastic Distinction in the Kinetic Profiles. *Chem. Commun.* **2011**, *47* (22), 6275−6277.